

# Noise generation by the interaction between ingested turbulence and a rotating fan

By S. J. MAJUMDAR<sup>†</sup> AND N. PEAKE

Department of Applied Mathematics and Theoretical Physics, University of Cambridge,  
Silver Street, Cambridge, CB3 9EW, UK

(Received 11 February 1997 and in revised form 18 November 1997)

An important criterion in the development of modern aeroengines is the identification of the dominant noise sources under typical aircraft take-off and approach conditions, and also in ground-based tests in which the engine is stationary. In this paper, we develop a theoretical model for *unsteady distortion noise*, which results from the interaction of ingested atmospheric turbulence with the rotating fan, with a view to providing a better understanding of the important physical mechanisms in this particular aspect of sound generation. The theory, developed in the frequency domain, is applicable for any arbitrary spectral form of atmospheric turbulence upstream of the fan, and as a simple model we take the von Kármán spectra for isotropic turbulence. The key fluid dynamical process in unsteady distortion is the deformation of turbulent eddies into long, narrow filaments as they enter the engine, due to the strong streamtube contraction experienced by the steady, non-uniform mean flow generated by the fan. Simple models of the steady flow fields are provided for both open and ducted rotor geometries. The distorted turbulent field at the fan face can be obtained using rapid distortion theory, and considerable simplification is made here by noting that the number of blades in typical aeroengine fans is large, allowing the application of asymptotic analysis and the derivation of closed-form expressions for those parts of the turbulence spectrum at the fan face which dominate the radiation. The unsteady forces exerted on the rotating fan blades are then calculated via a strip-theory approach. The resulting sound scattered to the far field is then evaluated using asymptotic theory for open and ducted rotors. Results are presented in the form of frequency spectra for the turbulent field at the fan face, the blade forces and the radiated sound for typical testing and aircraft operating conditions. High tonal noise levels are obtained under static conditions, whereas the sound is generally broadband in flight. The dependence on turbulence parameters such as the integral lengthscale is highlighted.

---

## 1. Introduction

The problem of noise generation by modern aeroengines is of great importance to the surrounding environment, and increasingly severe mandatory noise certification levels have been imposed in many of the world's airports. A considerable amount of time and money is currently being expended by engine manufacturers in measuring and attempting to reduce the undesirable levels of sound. The typical noise certification conditions are during aircraft take-off and approach; however, it is both highly

<sup>†</sup> Present address: Department of Meteorology, The Pennsylvania State University, 503 Walker Building, University Park, PA 16802-5013, USA.

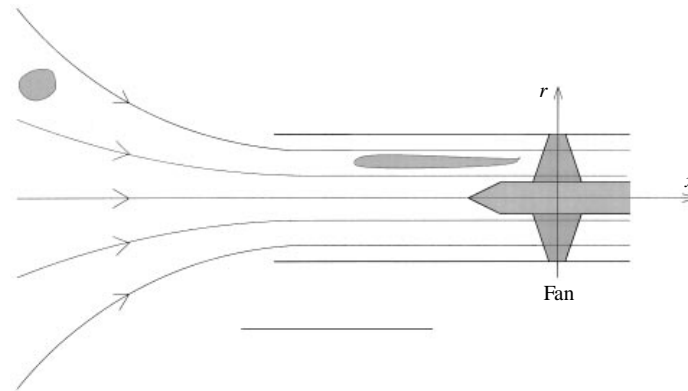


FIGURE 1. Engine configuration illustrating the inflow contraction and distortion of a turbulent eddy.

impractical and expensive to analyse the dominant noise sources in flight, and such noise testing must therefore be carried out for stationary engines at ground level. A difficulty exists in ground-based (static) tests since the dominant noise sources are different to those obtained in flight, and therefore further modifications must be made to the testing apparatus in order to realistically simulate flight and hence predict the expected noise levels under typical noise certification conditions. In static tests it has been deduced (e.g. Hanson 1974) that the dominant noise component arises from the interaction between ingested atmospheric turbulence and the engine fan which rotates at subsonic speeds, even when ambient wind speeds are low. The atmospheric turbulence component at the fan is termed *unsteady distortion* and in this paper we focus on the understanding of the physical processes that are responsible for the noise generated due to unsteady distortion–rotor interaction, by developing a theoretical prediction scheme.

The key physical mechanism in the unsteady distortion process is the elongation of turbulent eddies as they are convected towards the engine by the steady but non-uniform mean flow. A strong streamtube contraction exists immediately upstream of the fan, especially in static conditions, and it is this non-uniform inflow which causes the streamwise lengthscale of the turbulent eddies to increase significantly and the transverse scale to correspondingly decrease. The long, narrow filaments are accelerated through the fan, where they are consequently sliced a number of times by the fan blades. The repeated chopping produces an unsteady pressure distribution on the blades, which in turn generates sound which is scattered to the far field. In measured sound spectra, the peak noise levels occur at harmonics of the blade passing frequency (BPF), with the fundamental tone being of the highest magnitude. The engine geometry and an example of the distortion of a turbulent eddy are displayed in figure 1.

In flight, the streamtube contraction in the mean flow is expected to be far weaker than in static conditions (Cumpsty & Lowrie 1974), and hence the effects of unsteady distortion will be less significant. In fact, the dominant sound source in flight is thought to arise from ‘steady distortion’, i.e. an additional steady flow field such as that generated by non-uniformities (such as droop) in the engine inlet. Since the noise levels need to be quantified in flight, it is clear that the BPF tones obtained in static tests from unsteady distortion are highly undesirable. Various artificial mechanisms have therefore been introduced to remove the large-scale unsteady distortion components

at the fan face; however, the capability of such mechanisms to accurately produce a similar intake flow at the fan to that obtained in flight is still open to question. Further investigation of the effects of unsteady distortion under both static and flight conditions is therefore necessary, and since there are limits on how much knowledge can be gained by simply using practical measurements, a theoretical prediction scheme of the type to be described here for unsteady distortion would greatly enhance the overall level of knowledge in several aspects. It is important to develop a better understanding of the main fluid dynamical processes that occur upstream of the fan, with regard to the inflow contraction and distortion of the incoming turbulent eddies, and the nature of the acoustics in the far field.

The subject of noise generation by the interaction between turbulence and a rotating fan has received considerable attention in the past thirty years. One of the first works was by Sharland (1964), who developed a simple theory and experiments to estimate the noise generated by the interaction between turbulent flow and an airfoil. Subsequent improvements to the analytical and experimental work were made by Dean (1971). Alternative methods were developed by Mugridge (1970), Mani (1971) and Amiet (1975), which calculate the radiated sound from a combination of the inflow turbulence spectrum and the response function for a rectilinear airfoil. The first theoretical treatment of turbulence interacting with a rotating airfoil was developed by Homicz & George (1974), who calculated the airfoil pressures using a low-frequency response function and subsequently evaluated the pressure field of a rotating dipole source. Amiet (1977) used a different approach to calculate the sound field from a rotating blade source, by performing the rectilinear motion analysis of Amiet (1975) to yield expressions for the spectra at the fan. This model was particularly suited to high frequencies, whereas that of Homicz & George was only applicable to low frequencies.

The above models all characterized the turbulence at the fan as isotropic, i.e. the lengthscales were taken to be equal in both the streamwise and transverse directions. Cumpsty & Lowrie (1974) and Hanson (1974) were amongst the first to attempt to include the elongation of turbulent eddies (and hence their anisotropic nature) as they are drawn towards the fan. Using measurements of the turbulent flow in the inlet and the surface pressures on the blades, Hanson developed a theoretical model that was able to predict sound levels under static conditions. This involved a random-pulse-modulation theory to calculate the unsteady blade forces and hence the radiated sound arising from a statistical distribution of discrete eddies, whose characteristics were chosen in such a way that the shape of the theoretical blade lift spectrum agreed as closely as possible with that obtained experimentally. A more detailed theory of fan tone noise was developed by Ganz (1980), who paid particular attention to the modelling of free-stream turbulence (see §2.1) and the application of rapid distortion theory to obtain the turbulence characteristics downstream of the inflow contraction. Ganz represented the turbulent field by a statistical distribution of distortion elements and, using two-dimensional blade loading theory for single airfoils, the forces on the fan and scattered sound were calculated. The most comprehensive analytical study involving unsteady distortion theory was performed by Simonich *et al.* (1986, 1990) who applied rapid distortion theory to evaluate the noise generated by a helicopter rotor. Using an isotropic turbulence model in the free stream, Simonich *et al.* analysed the evolution of the turbulence as it travels along the contracting flow towards the rotor, under several typical helicopter operating conditions.

The conventional analytical model used to represent the evolution of the turbulent flow as it passes through the streamtube contraction is rapid distortion theory, which

forms an essential part of our analysis. Initial investigations on the subject of turbulent flow in a contracting stream were conducted by Prandtl (1933) and Taylor (1935). The now conventional rapid distortion theory approach was devised by Ribner & Tucker (1953), and Batchelor & Proudman (1954), who treated the turbulent field as a vorticity perturbation in the presence of a steady mean flow and hence were able to perform a linear analysis to determine the form of vorticity components as they travelled along contracting mean flow streamlines. Hunt (1973) extended these works to include Lighthill's (1956) *drift time*, defined by the time taken for a fluid particle to traverse along a mean flow streamline from an upstream point to a downstream point. The differences in drift time between fluid particles passing through the flow contraction were shown by Hunt to be significant. Hunt (1978) also published a review of the basic theory and its applicability. Goldstein (1978) reformulated the rapid distortion theory approach by splitting the perturbation flow field into a known vorticity field (with zero pressure perturbation) and an unknown irrotational component, in order to derive a single equation of Poisson form for the irrotational part, thereby providing a considerable simplification over previous studies. In this paper, we will apply the theory of Goldstein (1978) to calculate the velocity field of a distortion element as it passes through the contracting mean flow, and by linearity the result will then be generalized to any arbitrary form of free-stream turbulence.

The theory described in this paper is divided into several distinct stages, each of which can be modified and improved in a straightforward manner, whilst still remaining compatible with the rest of the theory. It is most convenient to work entirely in the frequency domain, which enables spectral expressions for the upstream turbulence, blade pressures and radiated sound to be derived. The present work represents a significant improvement over previous unsteady distortion noise models (e.g. Hanson 1974; Ganz 1980), in that we work directly with the upstream turbulence spectrum, so that there is no need to prescribe an artificial distribution of discrete eddies at the fan face to calculate the blade forces.

In §2, the theory is developed for an open rotor. The simple model for atmospheric turbulence which will be used throughout our theory is described, and expressions for the non-uniform steady flow upstream of the fan are provided. The rapid distortion theory approach formulated by Goldstein (1978) is applied to provide expressions for the distorted field at the fan face as a summation over azimuthal modes. In rapid distortion theory the unsteady velocity is decomposed as a sum of a vortical component, which is given analytically, and an irrotational component which can only be determined by solving an inhomogeneous Laplace equation; for general values of the azimuthal order,  $m$ , this Laplace equation can only be solved numerically. However, we show that provided the number of blades,  $B$ , in the fan is large (which is always true in practice), then apart from at unimportant low frequencies the radiation spectrum is dominated by contributions from those azimuthal modes with  $|m|$  close to a non-zero integer multiple of  $B$ . For these large values of  $m$ , it turns out to be possible to determine a closed-form expression for the irrotational part of the distorted field, and hence for those parts of the total distorted field which dominate the radiation. A two-dimensional theory to predict the unsteady blade response is then applied, and spectral expressions for the forces are deduced. Finally, we calculate the noise radiated to the far field using a Green's function approach and asymptotic theory. Extensions to our theory for a ducted rotor are presented in §3. The steady flow into a rotor surrounded by a semi-infinite cylindrical duct is evaluated using the Wiener-Hopf technique (Noble 1958). We use the identical rapid distortion theory

approach to that of §2 to evaluate the distorted field at the fan face, the only main difference being the imposition of a zero normal velocity boundary condition at the duct wall. An estimate of the total sound propagating back upstream is also provided using the Green's function for a cylindrical duct. Results are presented in §4 for typical engine testing conditions and in flight, for a wide range of parameters. Frequency spectra of the distorted field at the fan face, the unsteady blade forces and the radiated power are displayed, and the physical effects in both ground-based testing and flight conditions are deduced. The dominant noise level is observed at the blade passing frequency, with further peak levels occurring at higher harmonics. The dependence on the integral lengthscale of the free-stream turbulence is highlighted, and it is deduced that under static conditions eddies of larger lengthscale produce far greater tonal noise, whereas those of very small lengthscales produce effects not dissimilar to those predicted in flight conditions.

## 2. Formulation for an open rotor

### 2.1. Free-stream turbulence

In order to calculate the sound generated by the interaction of atmospheric turbulence with the fan, the turbulent flow field at the fan needs to be quantified. However, measured data for turbulence fields at the engine inlet or fan in static conditions are scarce, and in-flight measurements are impractical. It is therefore necessary to implement a realistic model of the spectrum of the atmospheric turbulence in the free field, from which the distortion of turbulent eddies as they approach the fan can be calculated using rapid distortion theory. A full and completely reliable description of turbulent fields in typical atmospheric conditions is not yet available, and an approximate model must therefore be chosen. Although atmospheric turbulence is not truly isotropic, its one-dimensional spectra (see Goldstein 1978) exhibit characteristics of isotropic turbulence with  $k^{-5/3}$  decay as the wavenumber  $k$  becomes large, and the flow is therefore taken to be locally isotropic within our wavenumber range of interest. It is generally agreed (e.g. Simonich *et al.* 1986) that the most realistic and convenient description of isotropic turbulence is represented by the von Kármán model. It is assumed that the flow is stationary and that the statistical properties of the unsteady flow field do not vary during the timescales of interest. Far upstream of the fan, the turbulent flow is also taken to be homogeneous in any horizontal plane, which is a reasonable assumption if the terrain height does not vary rapidly with respect to horizontal distance.

We consider a turbulence field superimposed on a free stream of velocity  $\hat{\mathbf{i}}U_\infty$  at upstream infinity (where  $\hat{\mathbf{i}}$  is the unit vector in the axial direction), so that the turbulent velocity is expressed as

$$\mathbf{u}^\infty(\mathbf{x} - \hat{\mathbf{i}}U_\infty t), \quad (2.1)$$

and we define the spatial correlation tensor in the form

$$R_{ij}^\infty(\boldsymbol{\eta}) = \langle u_i^\infty(\mathbf{x}) u_j^\infty(\mathbf{x} + \boldsymbol{\eta}) \rangle, \quad (2.2)$$

and the associated three-dimensional spectrum for the free-stream turbulence

$$S_{ij}^\infty(\mathbf{k}) = \frac{1}{(2\pi)^3} \int_{\mathfrak{R}^3} R_{ij}^\infty(\boldsymbol{\eta}) \exp(-i\mathbf{k} \cdot \boldsymbol{\eta}) \, d^3\boldsymbol{\eta}. \quad (2.3)$$

In our theory we will need to make use of the three-dimensional spectra for free-

stream turbulence  $S_{ij}^\infty(\mathbf{k})$  as defined in (2.3), since the spectral quantities derived later in our analysis will be obtained in the form of integral expressions dependent on  $S_{ij}^\infty(\mathbf{k})$ . The three-dimensional spectrum for the von Kármán model of isotropic turbulence is then given by (Hinze 1959; Amiet 1975; Goldstein 1978)

$$S_{ij}^\infty(\mathbf{k}) = \frac{55}{36\pi L^{2/3}} \frac{g_1 \overline{u_{\infty,1}^2} [k^2 \delta_{ij} - k_i k_j]}{(g_2/L^2 + k^2)^{17/6}}, \quad (2.4)$$

where the constants are  $g_1 \approx 0.1955$  and  $g_2 \approx 0.558$ . Two important parameters are apparent in this spectral expression: the integral lengthscale of the turbulence  $L$  and the mean square speed (i.e. the turbulence intensity) in the streamwise direction,  $\overline{u_{\infty,1}^2}$ .

Throughout our analysis we will be working with an axisymmetric flow geometry, so that the azimuthal component of the (non-uniform) mean flow is zero. We use the subscripts 1, 2, 3 to represent quantities calculated in the Cartesian system, and  $x, r, \theta$  to represent those in the cylindrical geometry. The 1- and  $x$ -axes coincide, and throughout this paper the quantities with these subscripts are interchangeable. There are nine non-zero components of  $S_{ij}^\infty(\mathbf{k})$  that describe the turbulent field in a general flow geometry. The axisymmetric nature of the base flow considered in this paper implies that only four such components  $S_{xx}^\infty, S_{rr}^\infty$  and  $S_{xr}^\infty = S_{rx}^\infty$  are required for subsequent calculations, and our results will therefore be independent of the azimuthal velocity components of the turbulent field.

## 2.2. The basic steady flow field

We now calculate the non-uniform steady flow induced by the rotating fan in the absence of the engine duct, in order to model the flow contraction that leads to the turbulence distortion. For the problem considered here, the flow is assumed to be axisymmetric, and hence effects of swirl upstream of the fan are neglected. It is therefore possible to work strictly in terms of the axial and radial coordinates  $x$  and  $r$ , with no dependence on the azimuthal angle  $\theta$ . The steady flow field  $\mathbf{U}(\mathbf{x})$  possesses axial and radial components

$$U_x = U_\infty + u(x, r), \quad U_r = v(x, r) \quad (2.5)$$

respectively, where  $U_\infty$  is the uniform free-stream axial speed at upstream infinity and  $(u, v)$  is the induced velocity field with  $(u, v) \rightarrow 0$  as  $x \rightarrow -\infty$ . A simple model which provides analytical expressions for the flow induced by a uniformly loaded *actuator disk* (i.e. an infinitely bladed propeller) is presented in Hough & Ordway (1965) and extended by Conway (1995). Expressions for the steady velocity components  $(u, v)$  and the streamfunction  $\Psi(x, r)$  are given in Appendix A. The use of an actuator disk to represent the fan is a very common device in turbomachinery theory, and captures all the essential features of the fan flow.

The calculated basic flow streamlines in typical static and flight conditions are displayed in figures 2(a) and 2(b) respectively. In both examples the same uniform flow speed  $U_f$  is prescribed at the fan face, since in practice the mean flow in static testing conditions is adjusted to simulate flight as closely as possible. It is observed that under static conditions the streamtube radius is approximately 10 times the order of that of the actuator disk and the contraction is therefore very strong, particularly near the tip of the actuator disk. Downstream of the actuator disk, the flow becomes parallel as required. In flight, the streamtube contraction is far weaker, and the steady flow upstream is parallel up to the close vicinity of the actuator disk. The effects of these representative flow fields on the distortion of the turbulent field will be

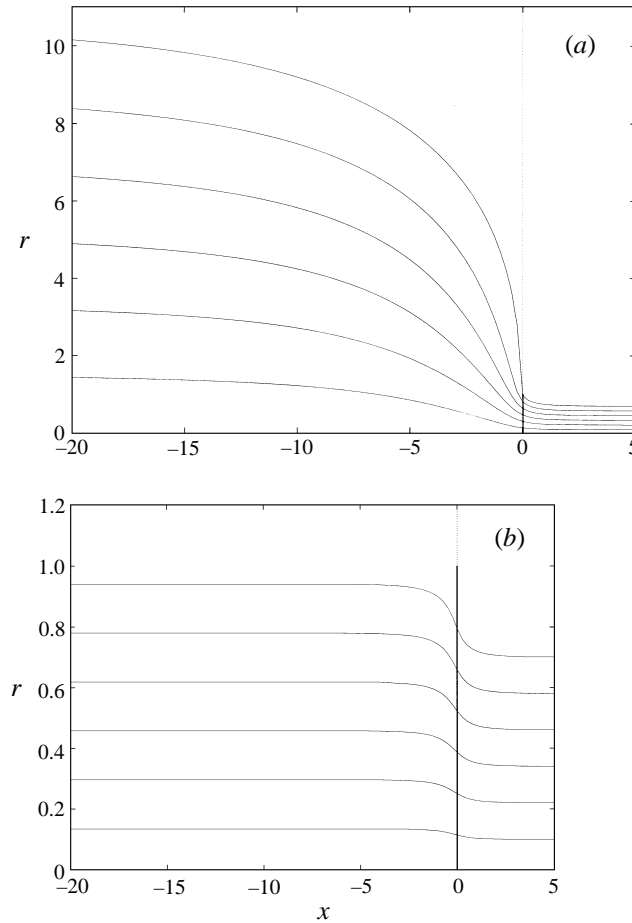


FIGURE 2. (a) Streamlines for the basic steady flow induced by an actuator disk of unit radius (situated at  $x = 0$ ) under typical static conditions. (b) Basic flow streamlines for an open rotor under typical aircraft approach conditions. Flow is from left to right.

calculated in the next subsection. It should be noted that the case of  $U_\infty = 0$  is of little practical relevance and is not considered in this paper, so that a non-zero upstream flow is present in both cases shown in figure 2.

### 2.3. Rapid distortion theory

One of the most important processes in the interaction of a rotating fan with convected turbulence is the distortion of the turbulent field as it is drawn towards the fan, and this depends upon the strength of the streamtube contraction in the basic steady flow. We consider an arbitrary turbulence field of the form  $\mathbf{u}^\infty(\mathbf{x} - \hat{\mathbf{i}}U_\infty t)$ , convected by a steady, axisymmetric mean flow  $\mathbf{U}(\mathbf{x})$  as presented in §2.2 for an unducted fan (and as will be seen later in §3.1 for a ducted fan). The flow is inviscid and incompressible (since the flight Mach number at aircraft approach is in the very low subsonic range), and we look for small unsteady perturbations, denoted by  $\mathbf{u}(\mathbf{x}, t)$ ,  $p'(\mathbf{x}, t)$ ,  $\rho'(\mathbf{x}, t)$ , to the basic steady flow velocity, pressure and density  $\mathbf{U}(\mathbf{x})$ ,  $p_0$ ,  $\rho_0$ .

The mean flow  $\mathbf{U}(\mathbf{x})$  is taken to be free of swirl upstream of the rotor throughout the analysis, and we can therefore work in an axisymmetric geometry, and introduce

a new cylindrical coordinate system  $\mathbf{X} = (X, R, \Theta)$ , in which the quantities  $X - U_\infty t$ ,  $R$  and  $\Theta$  are constant along the streamlines of the basic flow. The quantities  $X$  and  $R$  are the new ‘axial’ and ‘radial’ coordinates respectively, and  $\Theta$  is identically  $\theta$  in our axisymmetric system. The associated mean flow streamfunction is denoted by  $\Psi(\mathbf{x})$ . An important quantity in the analysis is Lighthill’s (1956) drift function  $\Delta(\mathbf{x})$ ; the difference in  $\Delta(\mathbf{x})$  between any two points on a streamline represents the time taken for a fluid particle to travel between the two positions, and it is defined by

$$\Delta(x, r) = \frac{x}{U_\infty} + \int_{-\infty}^x \left[ \frac{1}{U_x(x', r_s(x', R))} - \frac{1}{U_\infty} \right] dx', \quad (2.6)$$

where  $r_s(x', R)$  represents the equation of the streamline with constant value of  $R$  along it. The coordinates in our new system are given by

$$X = U_\infty \Delta, \quad R = \left( \frac{2\Psi}{U_\infty} \right)^{1/2}, \quad \Theta = \theta. \quad (2.7)$$

Now that we have constructed the basic flow field and the associated coordinate transformation, we proceed to apply the main result of Hunt’s (1978) and Goldstein’s (1978) theory. It has been shown that the general solution to the linearized momentum equation can be written in the form

$$p' = -\rho_0 \frac{D_0 \phi}{Dt}, \quad (2.8)$$

$$\mathbf{u} = \nabla \phi + \mathbf{u}^{(I)}, \quad (2.9)$$

where the function  $\phi(\mathbf{x}, t)$  satisfies the inhomogeneous equation

$$\nabla^2 \phi = -\nabla \cdot \mathbf{u}^{(I)}, \quad (2.10)$$

and  $\mathbf{u}^{(I)}(\mathbf{x})$  (using the notation of Goldstein 1978) is given by

$$\mathbf{u}_i^{(I)}(\mathbf{x}) = \mathcal{A}(\mathbf{X} - \hat{\mathbf{i}}U_\infty t) \cdot \frac{\partial \mathbf{X}}{\partial x_i}, \quad (2.11)$$

where  $\mathcal{A}$  is an arbitrary vector function. The quantity  $\mathbf{u}^{(I)}(\mathbf{x})$  is taken as known in the analysis, and it represents the vortical part of the disturbance field, with no associated pressure fluctuations. The irrotational part of  $\mathbf{u}$  can be evaluated as a gradient of the velocity potential  $\phi(\mathbf{x}, t)$ .

If we have a general incident disturbance field  $\mathbf{u}^\infty(\mathbf{x} - \hat{\mathbf{i}}U_\infty t)$  at upstream infinity, then by linearity the solution of (2.10) can be obtained by superposing solutions to the much simpler problem for an incident harmonic gust of form

$$\mathbf{u}^\infty = \mathbf{a} \exp\{\mathbf{i}\mathbf{k} \cdot (\mathbf{x} - \hat{\mathbf{i}}U_\infty t)\}, \quad (2.12)$$

where  $\mathbf{k} = (k_1, k_2, k_3)$  is the wavenumber vector at upstream infinity, and hence we take

$$\mathcal{A}(\mathbf{X}) = \mathbf{a} \exp(\mathbf{i}\mathbf{k} \cdot \mathbf{X}). \quad (2.13)$$

Even with this simplification, it is not possible to solve (2.10) analytically to determine  $\phi(\mathbf{x}, t)$  in closed form, and in general this would have to be completed numerically. However, we find that (2.10) can be solved asymptotically in the entirely realistic limit of large blade number,  $B$ ; the use of large- $B$  asymptotics in propeller aeroacoustics is fully described in Parry & Crighton (1989) and Crighton & Parry (1991). In this limit it turns out that for the radiation frequencies of most practical interest (but not



for the low frequencies, which are less important), the wavenumber vector  $\mathbf{k}$  and the distortion vector  $\mathbf{X}$  satisfy

$$|\mathbf{k}| \gg \frac{1}{|\mathbf{X}|}, \quad (2.14)$$

and this point will be justified fully at the end of this subsection and at the end of §2.5. This then allows us to write down the asymptotic solution

$$\phi(\mathbf{x}, t) = \frac{i l_m}{|\mathbf{l}|^2} \frac{\partial X_j}{\partial x_m} a_j \exp\{i \mathbf{k} \cdot (\mathbf{X} - \hat{\mathbf{i}} U_\infty t)\} \quad (2.15)$$

where  $\mathbf{l}$  is the local, distorted wavenumber

$$l_i = k_m \frac{\partial X_m}{\partial x_i}, \quad (2.16)$$

and to leading order in  $|\mathbf{k}|$  it is easy to see that this is indeed the solution (2.10) (essentially because to obtain the leading-order terms one differentiates the phase of  $\phi(\mathbf{x}, t)$  and not the amplitude). It then follows that the distorted field in this limit is given by

$$u_i(\mathbf{x}, t) = A_{ij} a_j \exp\{i \mathbf{k} \cdot (\mathbf{X} - \hat{\mathbf{i}} U_\infty t)\} \quad (2.17)$$

where

$$A_{ij}(\mathbf{x}; \mathbf{k}) = \left( \delta_{im} - \frac{l_i l_m}{|\mathbf{l}|^2} \right) \frac{\partial X_j}{\partial x_m}. \quad (2.18)$$

The distorted field (2.17) is now rewritten in cylindrical coordinates as a sum of its circumferential harmonics, using Formula 8.511.4 of Gradshteyn & Ryzhik (1980). Since  $A_{ij}$  is not a function of  $\theta$  (i.e. there is no rotation of the wavenumber vector due to the radial gradient of  $X$ ), it can be expressed in the form

$$u_i(\mathbf{x}, t) = \sum_{m=-\infty}^{\infty} B_{ij}^m(\mathbf{x}; \mathbf{k}) a_j \exp\left(ik_1(X - U_\infty t) + im\left(\theta - \tan^{-1}\left(\frac{k_3}{k_2}\right) + \frac{\pi}{2}\right)\right), \quad (2.19)$$

where

$$B_{ij}^m(\mathbf{x}; \mathbf{k}) = A_{ij}(\mathbf{x}; \mathbf{k}) J_m(k_r R) \quad (2.20)$$

and  $k_r = (k_2^2 + k_3^2)^{1/2}$  is the radial wavenumber. We therefore have an expression which describes the alteration of the amplitude and phase of the disturbance as it passes through the inflow contraction towards the fan. We note that expression (2.19) decays like  $r^{-1/2}$  at infinity, since  $R \rightarrow r$  far upstream and  $|J_m(z)| \propto [2/(\pi z)]^{1/2}$  as  $|z| \rightarrow \infty$ .

The distorted wavenumber vector  $\mathbf{l}(x, r) \equiv (l_x, l_r)$  contains the important information about the strength of the distortion and its effect on the axial and radial components of the wavenumber  $\mathbf{k} \equiv (k_x, k_r)$  of the harmonic disturbance at upstream infinity. From the definition (2.6) of the drift function, it would appear most convenient to express  $\Delta$  as a function of  $x$  and  $R$ , and from (2.16) we obtain expressions for the axial and radial components of  $\mathbf{l}(x, r)$  in the form

$$\left. \begin{aligned} l_x &= \left( k_r + k_x \frac{\partial}{\partial R} (U_\infty \Delta) \Big|_x \right) \frac{\partial R}{\partial x} \Big|_r + k_x \frac{\partial}{\partial x} (U_\infty \Delta) \Big|_r, \\ l_r &= \left( k_r + k_x \frac{\partial}{\partial R} (U_\infty \Delta) \Big|_x \right) \frac{\partial R}{\partial r} \Big|_x. \end{aligned} \right\} \quad (2.21)$$

The streamfunction and drift function, together with their axial and radial derivatives, must be evaluated using (2.6) and (2.7). It is clear from (2.7) that  $R \rightarrow r$  at upstream infinity for each streamline, since  $(u, v)$  tends to zero and therefore  $\Psi \sim \frac{1}{2}U_\infty r^2$ . It is easy to see from (2.7) that the derivatives of the streamfunction coordinate  $R$  take the form

$$\left. \frac{\partial R}{\partial r} \right|_x = \frac{rU_x}{RU_\infty}, \quad \left. \frac{\partial R}{\partial x} \right|_r = -\frac{rU_r}{RU_\infty}, \quad (2.22)$$

and the partial  $x$ -derivative of the coordinate  $X(x, R)$  is also straightforward to evaluate, and from (2.6) is given by

$$\left. \frac{\partial}{\partial x}(U_\infty \Delta) \right|_R = \frac{U_\infty}{U_\infty + u(x, r)}. \quad (2.23)$$

However, the most complicated derivative in (2.21) is the  $R$  derivative of  $\Delta$ , and the derivation of an analytical expression is given in Appendix B. Its final form is

$$\left. \frac{\partial}{\partial R}(U_\infty \Delta) \right|_x = U_\infty^2 R(x, r) \int_{-\infty}^x \frac{-r_s^{-5/2} \partial f / \partial r_s + \frac{3}{2} r_s^{-7/2} f(x', r_s)}{[U_\infty + u(x', r_s)]^3} dx', \quad (2.24)$$

where  $f(x', r_s)$  and  $\partial f / \partial r_s$  are given in Appendix B. It is noteworthy that the drift time varies significantly along the blade span in static conditions, and hence the expression (2.24) cannot be neglected. However, the drift possesses little significant radial variation in flight conditions.

It is now possible to evaluate the frequency spectrum of the turbulence after the streamtube contraction, in terms of the spectrum of the free-stream turbulence. We extend (2.12) to an arbitrary upstream turbulence field by linear superposition, and after a considerable amount of algebra we obtain the spectrum tensor averaged over all azimuthal angles in the simple form

$$S_{ij}^m(\mathbf{x}; \omega) = \frac{4\pi^2}{U_\infty} \int_0^\infty B_{ik}^m(\mathbf{x}; \mathbf{k}) B_{jl}^m(\mathbf{x}; \mathbf{k}) S_{kl}^\infty(\mathbf{k}) k_r dk_r, \quad (2.25)$$

in which the frequency  $\omega$  is related to the axial wavenumber  $k_x$  by

$$\omega = k_x U_\infty. \quad (2.26)$$

Examples of the spectra for the turbulent field at the fan face will be presented and discussed in §4.2. The derivation of (2.25) is presented in Appendix C, and similar manipulations are performed in §§2.4 and 2.5 to calculate the spectra of the unsteady blade forces and the radiated power.

At this point we are now able to justify our assumption (2.14) that  $|\mathbf{k}| \gg 1/|\mathbf{X}|$ . We first note that the number of blades,  $B$ , in typical aeroengine fans is large (usually between 20 and 30). Moreover, it will be seen at the end of §2.5 that the far-field radiation spectrum is dominated by contributions from azimuthal harmonics of the incident field whose order,  $m$ , is equal to a negative integer-multiple of  $B$  (i.e. in the notation of §2.5,  $m = -lB$  with  $l = 0, 1, 2, \dots$ ), and that the azimuthal mode  $m$  only then makes a significant contribution to the radiation spectrum for frequencies in the neighbourhood of  $\omega = lB\Omega$ , where  $\Omega$  is the shaft rotation frequency. The case  $l = 0$  (and hence  $m = 0$ ) therefore corresponds to low frequencies, which are of little practical interest and can be ignored. We then need only consider the cases  $l = 1, 2, \dots$ , and since  $B$  is large it follows that for the azimuthal modes of interest  $|m|$  is large

as well. If we now consider the evaluation of the integral in (2.25) for large  $|m|$ , it has been shown in a related problem by Crighton & Parry (1991) that the integral is dominated by contributions from the neighbourhood of the value of  $k_r$  for which the argument,  $k_r R$ , of the Bessel function in (2.20) is equal to its order,  $m$ , i.e. for wavenumbers  $\mathbf{k}$  such that

$$k_r R = |m| \gg 1 . \quad (2.27)$$

It therefore follows that

$$|\mathbf{k}| = (k_r^2 + k_x^2)^{1/2} \gg \frac{1}{|\mathbf{X}|} = \frac{1}{(R^2 + U_\infty^2 \Delta^2)^{1/2}} , \quad (2.28)$$

which is exactly the condition used in obtaining  $\phi(\mathbf{x}, t)$  in (2.15). It must therefore be emphasized that the expressions for  $S_{ij}^m(\mathbf{x}; \omega)$  given in this section are only valid for large values of  $|m|$ , but that is precisely what will be required for our radiation calculations; determination of the turbulence spectrum for small  $m$  would require a numerical solution of (2.10), but that seems to be of less practical importance and need not be considered further here.

#### 2.4. Calculation of blade forces

Now that the distorted unsteady velocity field at the fan face has been evaluated we are in a position to calculate the unsteady forces on the fan blades resulting from the interaction between the turbulence and the fan – we again restrict attention to the large values of  $|m|$  for which the theory in the previous subsection has been developed. We use the mathematical formulation of Smith (1972) by implementing the numerical subroutine LINSUB (developed by Whitehead 1987) to calculate the blade response to an incoming vortical perturbation. An expression for the spectrum of the blade forces is then deduced, and we also derive the unsteady forcing term in the governing equation for the sound radiated to the far field, the solution of which will be described in §2.5.

The reader is referred to Smith (1972) for the full details of the formulation; we need only describe the key features here. A number of assumptions are made, each of which can be justified under typical fan operating conditions. The flow is taken to be subsonic at each radial station, i.e. the mean flow Mach number relative to the blade,  $M_r < 1$ , where  $M_r = (M_x^2 + z^2 M_t^2)^{1/2}$ , and  $M_x$  and  $M_t$  are the axial Mach number at the fan and the tip rotational Mach number respectively, and  $z$  is the fraction of the total span along the blade at which the particular radial station under consideration is located. The blades operate at zero incidence to the oncoming flow. All quantities related to the flow are identical on each blade, except for a constant phase angle between adjacent blades. All perturbations to the mean flow are taken to be small, and hence the theory is linear. The fan contains  $B$  equally spaced blades of chord length  $c$ , rotating with angular speed  $\Omega$ . The calculation of the blade response is performed at a fixed radial station  $r$  along the rotating fan, at which the fan is approximated by an infinite two-dimensional linear cascade of flat plates. As described in Smith (1972), two different forms of propagating wave are then obtained from the linearized governing equations. One solution is a vorticity wave which is convected downstream by the steady mean flow, and the other corresponds to irrotational pressure perturbations that propagate upstream and downstream of the cascade. The unsteady blade pressures are then evaluated numerically at a prescribed number of chordwise stations along each blade.

The dimensional value  $\mathcal{L}_m$  of the  $m$ th azimuthal harmonic of the blade pressure

jump is defined to be

$$\mathcal{L}_m = \rho_0 M_r^2 c_0^2 \Gamma_W \left( \frac{x - x_0(r)}{\cos \lambda}, r; \frac{(k_1 U_\infty - m\Omega)c}{M_r c_0}, -\frac{2m\pi}{B} \right), \quad (2.29)$$

where  $\Gamma_W$  (using the notation of Smith 1972) is the non-dimensional pressure jump across the blade due to an incident harmonic gust. The first and second arguments correspond to the distance along the chord from the leading edge and the radial coordinate in our flow geometry, where the leading edge is situated at  $x = x_0(r)$  and  $\lambda$  is the blade stagger angle. The third and fourth arguments are the non-dimensional reduced frequency and the interblade phase angle respectively. The unit normal to the blade surface is denoted by  $\mathbf{N}$ , which is given in  $(x, r, \theta)$  coordinates by

$$\mathbf{N} = (\sin \lambda, 0, \cos \lambda). \quad (2.30)$$

To obtain the unsteady pressure jump across the blade due to the incoming distorted field calculated in §2.2, we must transform to a coordinate system fixed to the rotating fan. This is simply done by replacing  $(x, r, \theta)$  with  $(x, r, \theta')$  where  $\theta' = \theta - \Omega t$ , so that for the  $n$ th blade the leading edge is situated at  $x = x_0(r)$ ,  $\theta' = \theta_0(r) + 2n\pi/B$ ; here  $\theta_0(r)$  is the azimuthal position of the zeroth leading edge at time  $t = 0$ . By taking spatial Fourier transforms of the upstream unsteady velocity, and then using (2.19) to give the distorted form of each harmonic component at the fan face, the pressure jump arising from a free-stream disturbance  $\mathbf{u}^\infty(\mathbf{x} - \hat{\mathbf{i}}U_\infty t)$  convected by the mean flow is then given by

$$\begin{aligned} \Delta p^{(n)}(x, r, t) = & \int_{\mathbb{R}^3} \int_{\mathbb{R}^3} \sum_{m=-\infty}^{\infty} \frac{1}{(2\pi)^3} \mathcal{L}_m N_p B_{pk}^m \frac{u_k^\infty(\mathbf{x}')}{M_r c_0} \exp\left(ik_1(X - U_\infty t) \right. \\ & \left. + im\left(\theta - \tan^{-1}\left(\frac{k_3}{k_2}\right) + \frac{\pi}{2}\right)\right) \exp(-i\mathbf{k} \cdot \mathbf{x}') d^3 \mathbf{x}' d^3 \mathbf{k}. \end{aligned} \quad (2.31)$$

Using a similar technique to that described in Appendix C, we can then obtain the spectrum of the unsteady blade pressures in the form

$$S_{\Delta p \Delta p}(\mathbf{x}; \omega) = \sum_{m=-\infty}^{\infty} \frac{4\pi^2}{U_\infty} \sin^2 \lambda |\mathcal{L}_m|^2 S_{xx}^m(\mathbf{x}; \omega) \quad (2.32)$$

for our axisymmetric geometry. A simple relation has therefore been established between the spectrum of the blade forces and the  $xx$ -component of the turbulence spectrum at the fan, which was itself derived in (2.25). The axial wavenumber  $k_x$  is given by

$$k_x = \frac{\omega + m\Omega}{U_\infty}, \quad (2.33)$$

and hence a series of lift pulses at integer multiples of the shaft rotational frequency  $\Omega$  is expected. Examples of the spectra for the unsteady blade forces will be presented in §4.3.

We now derive an expression for the unsteady force on the fluid due to the presence of the rotor, which will appear as the source term used in the calculation of the noise radiated to the far field. The force  $\mathbf{f}(\mathbf{x}, t)$  at any point in space  $\mathbf{x}$  due to an incident harmonic gust whose form is given in (2.12) is simply the sum of the unsteady pressure

jumps given in (2.31) as each blade passes through that point, and it is written as

$$\begin{aligned} \mathbf{f}(\mathbf{x}, t) = N \sum_{m=-\infty}^{\infty} \sum_{n=-\infty}^{\infty} \mathcal{L}_m \delta \left( r \left( \theta' - \theta_0(r) - \frac{2n\pi}{B} \right) - (x - x_0(r)) \tan \lambda \right) N_p B_{pk}^m \frac{a_k}{M_r c_0} \\ \times \exp \left[ i \left\{ k_1 X - (k_1 U_\infty - m\Omega)t + m \left( \theta_0(r) + \frac{2n\pi}{B} - \tan^{-1} \left( \frac{k_3}{k_2} \right) + \frac{\pi}{2} \right) \right\} \right], \end{aligned} \quad (2.34)$$

where the zeros of the argument of the delta function correspond to each occasion a blade passes through  $\mathbf{x}$ . Using the identity derived from Poisson's summation formula (Jones 1966, p. 137)

$$\sum_{n=-\infty}^{\infty} \exp(in\theta) \delta(\psi + \Delta n) = \frac{1}{|\Delta|} \sum_{l=-\infty}^{\infty} \exp\{i\psi(2l\pi - \theta)/\Delta\}, \quad (2.35)$$

and re-expressing (2.34) in non-rotating coordinates, we obtain the forcing term in the form

$$\begin{aligned} \mathbf{f}(\mathbf{x}, t) = N \sum_{l=-\infty}^{\infty} \sum_{m=-\infty}^{\infty} \frac{B}{2\pi r} \mathcal{L}_m \frac{N_p B_{pk}^m a_k}{M_r c_0} \exp \left[ i(m + lB) \left\{ \theta - \theta_0(r) - \frac{x - x_0(r)}{r} \tan \lambda \right\} \right] \\ \times \exp i \left\{ k_1 X - (k_1 U_\infty + lB\Omega)t + m \left( \theta_0(r) - \tan^{-1} \left( \frac{k_3}{k_2} \right) + \frac{\pi}{2} \right) \right\}. \end{aligned} \quad (2.36)$$

The expression for the acoustic forcing is now in a convenient form for the calculation of the scattered sound, which will be described in §2.5.

### 2.5. The radiated sound field

We now evaluate the sound radiated to the far field using the free-space Green's function for the convected wave equation, in which the inhomogeneous term is the force exerted by the rotor on the fluid, as derived in §2.4. We take coordinates fixed with the aircraft, and therefore we are required to solve the wave equation in a medium with uniform axial mean flow  $U_\infty$  to evaluate the acoustic pressure  $p(\mathbf{x}, t)$  in the far field. The wave equation then takes the form

$$\nabla^2 p - \frac{1}{c_0^2} \left( \frac{\partial}{\partial t} + U_\infty \frac{\partial}{\partial x} \right)^2 p = \nabla \cdot \mathbf{f}(\mathbf{x}, t), \quad (2.37)$$

and  $p(\mathbf{x}, t)$  is assumed to possess harmonic time dependence identical to the forcing term. The unsteady force  $\mathbf{f}(\mathbf{x}, t)$  at a point  $\mathbf{x}$  in the fluid was derived in §2.4, and we model this term as a dipole source in the far field. The inhomogeneous forcing term is therefore given by the divergence  $\nabla \cdot \mathbf{f}$  as shown in (2.37).

In order to predict the sound reaching the far field, we need to work in a frame in which the effective source defined in (2.36) is moving in a straight line with speed  $U_\infty$ . These far-field coordinates are written in a plane-polar geometry as  $(\sigma_0, \varphi)$ , where  $\sigma_0$  is the distance from the source centre (i.e. the centre of the fan) to the stationary observer at retarded (or emission) time  $\tau$ , and  $\varphi$  is the angle between the axis of the fan and the line joining the observer to the source centre as displayed in figure 3. The origin in  $(x, r)$  coordinates travels with the source at flight Mach number  $M_\infty$  relative to the observer, and our local cylindrical coordinate system is then expressed in terms of the far-field coordinates  $(\sigma_0, \varphi)$  in the form

$$r = \sigma_0 \sin \varphi, \quad x = -\sigma_0 \cos \varphi + M_\infty \sigma_0. \quad (2.38)$$

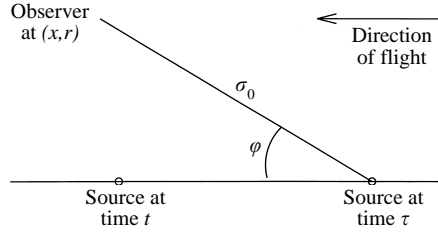


FIGURE 3. The far-field geometry. Sound is emitted at time  $\tau$ , and is heard by the observer at a later time  $t$ .

We now consider each azimuthal harmonic in (2.37) separately, and it can be shown (see Majumdar 1996 for further details) that in the far field ( $\sigma_0 \rightarrow \infty$ ), the Green's function for the  $n$ th azimuthal harmonic in (2.37) is

$$G_n(x, r; x_1, r_1) = -\frac{i}{4} \exp\left(-\frac{in\pi}{2} - \frac{i\pi}{2}\right) \frac{1}{2\sigma_0(1 - M_\infty \cos \varphi)} J_n(\gamma_0 r_1) \\ \times \exp\left(\frac{i\omega x_1 \cos \varphi}{c_0(1 - M_\infty \cos \varphi)}\right) \exp\left(-i\omega\left(t - \frac{\sigma_0}{c_0}\right) + in\theta\right) \quad (2.39)$$

where

$$\gamma_0 = \frac{\omega \sin \varphi}{c_0(1 - M_\infty \cos \varphi)}. \quad (2.40)$$

The far-field pressure measured by a stationary observer is then given by applying (2.39) to (2.37) and summing over all azimuthal modes, in the form

$$p(\mathbf{x}, t) = \frac{1}{(2\pi)^3} \sum_{l=-\infty}^{\infty} \sum_{m=-\infty}^{\infty} \int_{\mathbb{R}^3} \int_{\mathbb{R}^3} u_i^\infty(\mathbf{x}') \exp(-i\mathbf{k} \cdot \mathbf{x}') \int_0^c \int_0^{r_A} \mathcal{H}_i(x_1, r_1, l, m, \mathbf{k}) \\ \times \exp\left\{-i\omega\left(t - \frac{\sigma_0}{c_0}\right) + i(m + lB)\theta + im\left(\frac{\pi}{2} - \tan^{-1}\left(\frac{k_3}{k_2}\right)\right)\right\} dr_1 dx_1 d^3\mathbf{x}' d^3\mathbf{k}, \quad (2.41)$$

where the integrals over  $r_1$  and  $x_1$  are over the blade span and chord respectively, and it follows that for an arbitrary upstream vortical disturbance field  $\mathbf{u}^\infty(\mathbf{x} - \hat{\mathbf{i}}U_\infty t)$  the function  $\mathcal{H}_i$  takes the form

$$\mathcal{H}_i(x_1, r_1, l, m, \mathbf{k}) = \frac{J_{m+lB}(\gamma_0 r_1) B}{16\pi\sigma_0 M_r c_0 (1 - M_\infty \cos \varphi)} \exp\left(i\frac{(k_1 U_\infty + lB\Omega) \cos \varphi}{c_0(1 - M_\infty \cos \varphi)} x_1\right) \\ \times \exp\left[i\left\{k_1 X - lB\theta_0(r_1) - (m + lB)\left(\frac{x_1 - x_0(r_1)}{r_1} \tan \lambda + \frac{\pi}{2}\right)\right\}\right] \\ \times \mathcal{L}_m(x_1, r_1; \omega) N_p B_{pi}^m(x_1, r_1; k_r, \omega) \mathbf{D} \cdot \mathbf{N} \\ \equiv \mathcal{P}(x_1, r_1; \omega) \mathcal{L}_m(x_1, r_1; \omega) N_p B_{pi}^m(x_1, r_1; k_r, \omega), \quad (2.42)$$

and where

$$\mathbf{D} \equiv \left(\frac{-i\omega \cos \varphi}{c_0(1 - M_\infty \cos \varphi)}, 0, \frac{i(m + lB)}{r_1}\right) \quad (2.43)$$

in  $(x, r, \theta)$  coordinates. Note that  $p(\mathbf{x}, t)$  possesses the usual  $\sigma_0^{-1}$  dependence with distance, together with the Doppler factor  $(1 - M_\infty \cos \varphi)^{-1}$  in the phase due to the aircraft forward motion.

The spectrum for the far-field noise is calculated using a similar technique to that used to determine the post-contraction turbulence spectra (described in Appendix C), and the relevant expression for an observer at  $\mathbf{x}$  is given by

$$S_{pp}(\mathbf{x}, \omega) = \frac{2\pi}{U_\infty} \int_{\mathbb{R}^2} \sum_{l=-\infty}^{\infty} \sum_{m=-\infty}^{\infty} \int_{-\infty}^{\infty} \int_0^{\infty} \mathcal{H}_i^*(x'_1, r'_1, l, m, \mathbf{k}) \, dr'_1 \, dx'_1 \\ \times \int_{-\infty}^{\infty} \int_0^{\infty} \mathcal{H}_j(x_1, r_1, l, m, \mathbf{k}) \, dr_1 \, dx_1 \, S_{ij}^\infty(\mathbf{k}) \, dk_2 \, dk_3, \quad (2.44)$$

where

$$k_1 = k_x = \frac{\omega - lB\Omega}{U_\infty}, \quad (2.45)$$

and \* denotes the complex conjugate. From (2.42) we finally obtain

$$S_{pp}(\mathbf{x}; \omega) = \int_0^{\infty} \sum_{l=-\infty}^{\infty} \sum_{m=-\infty}^{\infty} \int_{-\infty}^{\infty} \int_0^{\infty} \mathcal{P}^*(x'_1, r'_1; \omega) \mathcal{L}_m^*(x'_1, r'_1; \omega) B_{xi}^m(x'_1, r'_1; k_r, \omega) \, dr'_1 \, dx'_1 \\ \times \frac{4\pi^2 \sin^2 \lambda}{U_\infty} \int_{-\infty}^{\infty} \int_0^{\infty} \mathcal{P}(x_1, r_1; \omega) \mathcal{L}_m(x_1, r_1; \omega) B_{xj}^m(x_1, r_1; k_r, \omega) \, dr_1 \, dx_1 \, S_{ij}^\infty(\mathbf{k}) \, k_r \, dk_r. \quad (2.46)$$

To obtain the total radiated power,  $P(\omega)$ , in the far field, the expression for  $S_{pp}(\mathbf{x}; \omega)$  is integrated over a spherical shell of radius  $\sigma_0$  to give

$$P(\omega) = 2\pi \sigma_0^2 \int_0^\pi S_{pp}(\sigma_0, \varphi; \omega) \sin \varphi \, d\varphi, \quad (2.47)$$

and it will prove convenient to consider the power level (PWL) in decibels, as in Dowling & Ffowcs Williams (1983), in the form

$$\text{PWL} = 10 \log_{10} \left( \frac{\text{sound power output } P(\omega)}{10^{-12} \text{ W}} \right). \quad (2.48)$$

The spectrum of the far-field radiation is expected to consist of peaks centred around  $\omega = lB\Omega$ ,  $l = 0, \pm 1, \pm 2, \dots$ , which corresponds to the frequency with which a turbulent eddy is chopped by the blades. This follows by first noting that the Bessel function  $J_{m+lB}$  in (2.42) will make its most significant contribution to the radiation spectrum when  $m$  is close to  $-lB$ , so that from (2.45) the axial wavenumber is then  $k_x \approx (\omega + m\Omega)/U_\infty$ . Also, since the von Kármán spectrum decays rapidly with increasing  $k_x$  (see figure 10*b*), it follows that the azimuthal mode  $m$  will only make a significant contribution when  $\omega \approx -m\Omega$ . These are precisely the facts used at the end of § 2.3 to derive the condition (2.14).

Results will be presented in § 4.4 illustrating the effects of turbulence lengthscale and inflow conditions. We again emphasize that (2.44) corresponds to radiation from an open rotor. In the next section we go on to predict the effects of the engine nacelle by considering a ducted rotor.

### 3. Formulation for a ducted rotor

The theory for unsteady distortion noise of the unducted fan is now extended to the case when the fan is surrounded by a nacelle. For the purposes of this analysis, the nacelle is modelled as a semi-infinite cylindrical duct, and the fan is placed sufficiently far downstream of the duct inlet that the flow is uniformly parallel at the fan face.

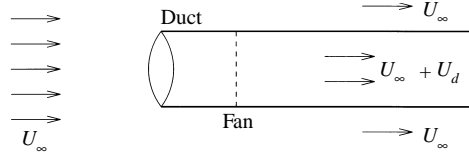


FIGURE 4. Geometry of system in which fan is placed inside a semi-infinite cylindrical duct.

### 3.1. Basic steady flow field

Consider a cylindrical duct with circular cross-section of radius  $a$ , which is semi-infinite in the positive  $x$ -direction. There is a uniform axial mean flow  $U_\infty$  at infinity outside the cylinder, but we suppose that far downstream inside the cylinder there is an additional flow  $U_d$ , so that the total flow speed downstream is  $U_\infty + U_d$ , see figure 4. This additional component  $U_d$  models the effect of the fan in accelerating the flow through the intake.

We consider inviscid, irrotational steady incompressible flow and use the Wiener–Hopf technique to solve the Laplace equation for the fluid velocity potential. Again, we can neglect compressibility in determining the steady flow, since the flight Mach numbers are low in the conditions of general interest. As is common in Wiener–Hopf methods applied to incompressible flow problems, we define a small parameter  $\epsilon$  for the purpose of analysis in Fourier-transform space, and look for solutions for the velocity potential  $\phi_t(x, r)$  that satisfy the equation

$$(\nabla^2 - \epsilon^2)\phi_t = 0; \quad (3.1)$$

at the end of the analysis we will send  $\epsilon \rightarrow 0$ . We write  $\phi_t(x, r)$  in the form

$$\phi_t(x, r) = \begin{cases} U_\infty x + U_d x + \phi(x, r), & r < a \\ U_\infty x + \phi(x, r), & r > a \end{cases} \quad (3.2)$$

and then take the Fourier transform in the streamwise direction  $x$ , defined by

$$\Phi(\alpha, r) = \int_{-\infty}^{\infty} \phi(x, r) e^{i\alpha x} dx, \quad (3.3)$$

of (3.1). The solution of this transformed equation which is non-singular on the axis  $r = 0$  and which decays at infinity is then easily expressed in terms of the modified Bessel functions as

$$\Phi(\alpha, r) = \begin{cases} A(\alpha) I_0(\kappa r), & r < a \\ B(\alpha) K_0(\kappa r), & r > a, \end{cases} \quad (3.4)$$

where

$$\kappa = (\alpha^2 + \epsilon^2)^{1/2}. \quad (3.5)$$

The complex  $\alpha$ -plane contains branch points at  $\pm i\epsilon$ , with the branch cuts taken to infinity in the upper and lower half-planes respectively. The quantity  $\kappa$  takes positive real values as  $\alpha \rightarrow \infty$  along the positive real axis.

We prescribe the following boundary conditions on the flow:

- (i) The radial velocity is continuous across  $r = a$  for all  $x$ , i.e.

$$\frac{\partial \phi_t}{\partial r} \text{ is continuous across } r = a. \quad (3.6)$$



(ii) The radial velocity is identically zero on the surface of the cylinder, giving

$$\frac{\partial \phi_t}{\partial r} = 0 \quad \text{on } r = a, \quad x > 0. \quad (3.7)$$

(iii) The axial velocity must be continuous across  $r = a$  for  $x < 0$ , so

$$\frac{\partial \phi_t}{\partial x} \text{ is continuous across } r = a, \quad x < 0. \quad (3.8)$$

In order to apply boundary condition (iii) we must first introduce an artificial damping factor into (3.2) by replacing  $U_d$  by  $U_d e^{\epsilon x}$ , in order to allow the transforms to be completed. We now multiply (3.2) by  $e^{i\alpha x}$  and integrate over  $x < 0$  to yield

$$[\phi(-0, a)] - i\alpha [\Phi(\alpha, a)]^- - \frac{U_d}{i\alpha + \epsilon} = 0, \quad (3.9)$$

where  $[\Phi(\alpha, a)]^-$  is simply the transform of the jump in  $\phi(x, r)$  across  $r = a$  over the negative half-range  $x < 0$ , and  $[\phi(-0, a)]$  is the jump in the potential across  $r = a$  at  $z = 0$ . We now take the  $r$ -derivative of (3.4) to yield a relationship between  $A(\alpha)$  and  $B(\alpha)$  from (i), while from boundary condition (ii) we see that

$$\frac{\partial \Phi}{\partial r}(\alpha, a) = \frac{\partial \Phi^-}{\partial r}(\alpha, a), \quad (3.10)$$

where  $(\partial \Phi / \partial r)^-(\alpha, a)$  is the transform of  $\partial \phi / \partial r$  over the negative half-range  $x < 0$ , which is then used to give an expression for  $A(\alpha)$  in terms of  $(\partial \Phi / \partial r)^-(\alpha, a)$ . By combining this result with (3.9), it is then a straightforward matter to obtain the equation

$$[\phi(-0, a)] = -i\alpha [\Phi(\alpha, a)]^+ + \frac{\partial \Phi^-}{\partial r}(\alpha, a) \frac{i\alpha}{\kappa^2 a I_0'(\kappa a) K_0'(\kappa a)} - \frac{iU_d}{\alpha - i\epsilon}, \quad (3.11)$$

where  $[\Phi(\alpha, a)]^+$  is the transform of the jump in  $\phi(x, r)$  across  $r = a$  over the positive half-range  $x > 0$ . We write the Wiener–Hopf kernel as

$$\mathcal{K}(\alpha) = -2I_0'(\kappa a) K_0'(\kappa a) = 2I_1(\kappa a) K_1(\kappa a) = \mathcal{K}^+(\alpha) \mathcal{K}^-(\alpha), \quad (3.12)$$

where  $\mathcal{K}^+(\alpha)$  and  $\mathcal{K}^-(\alpha)$  are analytic, free of zeros and possess algebraic behaviour at infinity in the upper and lower half-planes  $\mathcal{R}^\pm$ , defined by

$$\mathcal{R}^+ \equiv \{ \alpha : \text{Im}(\alpha) > -\epsilon \} \quad \text{and} \quad \mathcal{R}^- \equiv \{ \alpha : \text{Im}(\alpha) < \epsilon \} \quad (3.13)$$

respectively. The kernel  $\mathcal{K}(\alpha)$  is regular in the strip  $|\text{Im}(\alpha)| < \epsilon$ , and has the value unity at the branch points  $\alpha = \pm i\epsilon$ . Equation (3.11) is then rewritten in the Wiener–Hopf form

$$\begin{aligned} \alpha [\phi(-0, a)] \mathcal{K}^+(\alpha) + i\alpha^2 [\Phi(\alpha, a)]^+ \mathcal{K}^+(\alpha) + iU_d \alpha \left\{ \frac{\mathcal{K}^+(\alpha) - \mathcal{K}^+(i\epsilon)}{\alpha - i\epsilon} \right\} \\ = -2i \frac{\partial \Phi^-}{\partial r} \frac{1}{a \mathcal{K}^-(\alpha)} - iU_d \alpha \frac{\mathcal{K}^+(i\epsilon)}{\alpha - i\epsilon}, \end{aligned} \quad (3.14)$$

and since the left-hand and right-hand sides of (3.14) are analytic in  $\mathcal{R}^+$  and  $\mathcal{R}^-$  respectively, by analytic continuation they define a function which is analytic throughout the  $\alpha$ -plane. Moreover, in order to ensure that we obtain the least-singular solution, we insist that both sides of (3.14) approach zero as  $\alpha \rightarrow \infty$  in the respective half-plane.

By Liouville's theorem, it therefore follows that both sides of (3.14) are identically zero, from which we can determine an expression for the unknown  $(\partial\Phi/\partial r)^-(\alpha, a)$ . After some manipulation we find that

$$\Phi(\alpha, r) = -\frac{aU_d\alpha\mathcal{K}^-(\alpha)\mathcal{K}^+(i\epsilon)}{2(\alpha - i\epsilon)} \frac{I_0(\kappa r)}{\kappa I_0'(\kappa a)}, \quad r < a \quad (3.15)$$

$$\Phi(\alpha, r) = -\frac{aU_d\alpha\mathcal{K}^-(\alpha)\mathcal{K}^+(i\epsilon)}{2(\alpha - i\epsilon)} \frac{K_0(\kappa r)}{\kappa K_0'(\kappa a)}, \quad r > a, \quad (3.16)$$

and using the factorization technique described in Levine & Schwinger (1948), and Peake (1995), the expressions for the Wiener–Hopf factors  $\mathcal{K}^\pm(\alpha)$  are given by

$$\mathcal{K}^\pm(\alpha) = [2I_1(\kappa a)K_1(\kappa a)]^{1/2} \exp\left\{\pm\frac{\alpha}{\pi i} \int_0^\infty \frac{\ln[2I_1(ax)K_1(ax)]}{x^2 - \alpha^2} dx\right\}. \quad (3.17)$$

We can now set  $\epsilon = 0$  since the Wiener–Hopf factorization is complete, so that the term  $\kappa$  of (3.5) is simply equal to  $|\alpha|$ . We are now required to retrieve the velocity potential  $\phi(x, r)$  by inverting the Fourier transform (3.15), (3.16), and the solution takes different forms depending on the position relative to the duct.

(a)  $r < a$ , within the duct radius

The  $x$  and  $r$  derivatives of  $\phi(x, r)$  are taken to obtain the required velocity field components  $u(x, r)$  and  $v(x, r)$ . The integral expression for the axial speed  $u(x, r)$  possesses a simple pole at  $\alpha = i\epsilon$ , and we therefore obtain  $u(x, r)$  as a sum of the contribution from the pole and the Cauchy principal value in the form

$$u(x, r) = \frac{U_d}{2} + \frac{iaU_d}{2\pi} \text{P} \int_{-\infty}^{\infty} \frac{\alpha K_1(|\alpha|a)I_0(|\alpha|r)}{|\alpha|R(\alpha)} \exp(-i\alpha x + i\theta(\alpha)) d\alpha, \quad (3.18)$$

where from (3.17) we have written

$$\mathcal{K}^+(\alpha) = \mathcal{K}^-(-\alpha) = R(\alpha)e^{-i\theta(\alpha)}, \quad (3.19)$$

P indicates the Cauchy principal value and where we have now taken the limit  $\epsilon \rightarrow 0$  in the integral. Note that  $R(\alpha) = R(-\alpha)$ ,  $\theta(\alpha) = -\theta(-\alpha)$  and  $\mathcal{K}^\pm(0) = 1$ . Equation (3.18) exhibits the correct behaviour as  $|x| \rightarrow \infty$ , namely  $u(x, r) \rightarrow 0$  as  $x \rightarrow -\infty$  and  $u(x, r) \rightarrow U_d$  as  $x \rightarrow +\infty$ . The radial velocity  $v(x, r)$  is given by

$$v(x, r) = \frac{\partial\phi}{\partial r} = -\frac{aU_d}{\pi} \int_0^\infty \frac{K_1(\alpha a)I_1(\alpha r)}{R(\alpha)} \cos(\alpha x - \theta(\alpha)) d\alpha \quad (3.20)$$

and we note that no singularity exists in the integrand since  $K_1(\alpha a)I_1(\alpha r) \rightarrow r/2a$  as  $\alpha \rightarrow 0$ . The corresponding streamfunction  $\Psi(x, r)$  for  $r < a$  is expressed as

$$\Psi(x, r) = \frac{1}{2}U_\infty r^2 + \frac{1}{4}U_d r^2 + \frac{iaU_d r}{2\pi} \text{P} \int_{-\infty}^{\infty} \frac{\alpha K_1(|\alpha|a)I_1(|\alpha|r)}{|\alpha|^2 R(\alpha)} \exp(-i\alpha x + i\theta(\alpha)) d\alpha. \quad (3.21)$$

(b)  $r > a$ , outside the duct radius

In exactly the same way, the axial and radial velocity components are now given by

$$u(x, r) = -\frac{aU_d}{\pi} \int_0^\infty \frac{I_1(\alpha a)K_0(\alpha r)}{R(\alpha)} \sin(\alpha x - \theta(\alpha)) d\alpha, \quad (3.22)$$

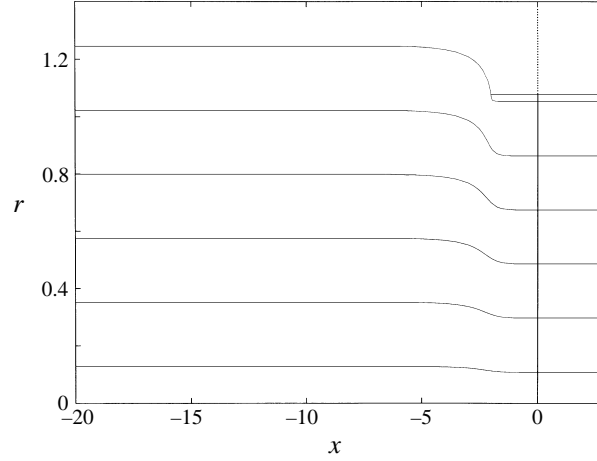


FIGURE 5. Streamlines of the flow induced by a sink downstream inside an infinite cylindrical duct in typical flight conditions, in which the ratio  $U_d/U_\infty = 0.412$ . The streamtube radius is roughly 1.2 times the duct radius. Flow is from left to right.

$$v(x, r) = -\frac{aU_d}{\pi} \int_0^\infty \frac{I_1(\alpha a)K_1(\alpha r)}{R(\alpha)} \cos(\alpha x - \theta(\alpha)) d\alpha, \quad (3.23)$$

and the streamfunction  $\Psi(x, r)$  is written in the form

$$\Psi(x, r) = \frac{1}{2}U_\infty r^2 + \frac{1}{4}U_d a^2 + \frac{iaU_d r}{2\pi} \mathbf{P} \int_{-\infty}^\infty \frac{\alpha I_1(|\alpha|a)K_1(|\alpha|r)}{|\alpha|^2 R(\alpha)} \exp(-i\alpha x + i\theta(\alpha)) d\alpha, \quad (3.24)$$

where the constant  $U_d a^2/4$  has been introduced to ensure continuity of  $\Psi$  across  $r = a$ . A plot of the basic-flow streamlines in typical aircraft approach conditions is displayed in figure 5. The flow is uniform and parallel at the fan face with speed  $U_f = U_\infty + U_d$ , and outside the duct a small streamtube contraction is observed, although only in the close vicinity of the duct. Away from the duct, the flow is parallel both upstream and downstream.

### 3.2. Rapid distortion theory

We use a similar formulation of rapid distortion theory to that described in §2.3, but this time using the basic steady flow  $\mathbf{U}(\mathbf{x})$  as calculated in §3.1. Again, we consider only azimuthal harmonics with  $|m|$  large, so that the closed-form expressions for the irrotational part of the distorted velocity field can still be used. However, the distorted velocity field as expressed in (2.19) does not satisfy the boundary condition of zero normal velocity on the wall of the cylinder, since the calculations in §2.3 are performed for an unducted rotor, and we must therefore include an additional term in the distorted field to render the radial flow to be zero on  $r = a$ . Firstly, we express the radial velocity component of the incident turbulent field from (2.19) in the form of a summation over the circumferential harmonics

$$u_r(\mathbf{x}, t) = \sum_{m=-\infty}^{\infty} \hat{r}_i B_{ij}^m(\mathbf{x}; \mathbf{k}) a_j \exp\left(ik_1(X - U_\infty t) + im\left(\theta - \tan^{-1}\left(\frac{k_3}{k_2}\right) + \frac{\pi}{2}\right)\right). \quad (3.25)$$

We now introduce an additional irrotational velocity to exactly cancel this radial component on  $r = a$ ; we look for  $\phi(x, r, t)$  as a solution of Laplace's equation in the

form

$$\phi(x, r, t) = f(r) \exp \left\{ ik_1(X - U_\infty t) + im \left( \theta - \tan^{-1} \left( \frac{k_3}{k_2} \right) + \frac{\pi}{2} \right) \right\} \quad (3.26)$$

for the  $m$ th circumferential harmonic. Since we suppose that the fan is placed sufficiently far downstream of the inlet for the mean flow at the fan to be parallel, the distorted axial wavenumber  $l_1$  is given by (using 2.21)

$$l_1 = \frac{\partial X}{\partial x} k_1, \quad (3.27)$$

where  $\partial X/\partial x$  is constant. Laplace's equation therefore reduces to the modified Bessel equation in  $r$ , which yields a solution that is non-singular on the axis. Setting the total normal velocity on the duct wall  $r = a$  to zero yields the solution for  $f(r)$  in the form

$$f(r) = -\frac{\hat{r}_i \bar{B}_{ij}^m a_j I_m(l_1 r)}{l_1 I_m(l_1 a)}, \quad (3.28)$$

where the overbar denotes that  $B_{ij}^m$  is evaluated at  $r = a$ . The field induced by the inflow distortion can then be written as

$$u_i = \sum_{m=-\infty}^{\infty} C_{ij}^m(r; \mathbf{k}) a_j \exp \left\{ ik_1(X - U_\infty t) + im \left( \theta - \tan^{-1} \left( \frac{k_3}{k_2} \right) + \frac{\pi}{2} \right) \right\}, \quad (3.29)$$

where  $C_{ij}^m$  can be calculated in full from (3.25) to (3.28). When the flow is axisymmetric, the  $\theta$ -components of  $C_{ij}^m$  are unnecessary, and the expressions for  $C_{ij}^m$  can be simplified by noting that

$$\hat{x}_i B_{ij}^m = B_{xj}^m \quad \text{and} \quad \hat{r}_i B_{ij}^m = B_{rj}^m, \quad (3.30)$$

and so we obtain

$$C_{rj}^m(r; \mathbf{k}) = B_{rj}^m - \bar{B}_{rj}^m \frac{I_m'(l_1 r)}{I_m'(l_1 a)}, \quad (3.31)$$

$$C_{xj}^m(r; \mathbf{k}) = B_{xj}^m - i \bar{B}_{rj}^m \frac{I_m(l_1 r)}{I_m'(l_1 a)}. \quad (3.32)$$

We are now in a position to calculate the distorted turbulence spectra, and we can simply perform the same analysis as in §2, since the velocity field (3.29) is of an equivalent form to that in (2.19) with  $C_{ij}^m(r; \mathbf{k})$  replacing  $B_{ij}^m(\mathbf{x}; \mathbf{k})$ . The expression for the post-contraction turbulence spectrum then takes the form

$$S_{ij}^m(\mathbf{x}; \omega) = \frac{4\pi^2}{U_\infty} \int_0^\infty C_{ik}^{m*}(r; \mathbf{k}) C_{jl}^m(r; \mathbf{k}) S_{kl}^\infty(\mathbf{k}) k_r dk_r \quad (3.33)$$

for the  $m$ th circumferential harmonic in our axisymmetric geometry, and in (3.33)  $k_x = \omega/U_\infty$ .

The calculation of the unsteady blade forces is unchanged from §2.4, with only the terms arising from the inflow distortion changing form due to the presence of the duct, so that the spectrum of the blade pressures is therefore given by (2.32) with  $S_{xx}^m$  taken from (3.33). The frequency in this case is given by  $\omega = k_x U_\infty - m\Omega$ .

### 3.3. The radiated sound field

For a ducted rotor, the radiated directivity is different to that calculated in §2.5 for the unducted rotor. However, the total sound power emitted by the ducted rotor will

be in close agreement with that emitted by the same rotor without the duct, essentially because for the many-bladed fans of practical interest most of the radiation is emitted at relatively high frequency, for which the reflection coefficients at either end of the cylindrical duct are very small. The ducted rotor will of course emit radiation both upstream and downstream, but clearly it is only the upstream radiation that escapes to the far field and needs to be included in a noise prediction scheme – the downstream component is for the most part attenuated within the engine. In order to estimate the sound power level for a ducted rotor, it therefore follows that we can simply calculate the emitted power as if the rotor were unducted, as in §2, and multiply this result by the fraction of the total power from a ducted rotor which propagates upstream. In this subsection we aim to estimate this fraction, and to do this we first consider a single point source located in an infinite duct at a radius  $r_1$  and axial coordinate  $x_1$ . The sound field in the duct is then given by the ducted Green's function, the  $n$ th azimuthal harmonic of which is denoted  $G_n(x, r; x_1, r_1)$ . By taking Fourier transforms in  $x$ , applying the zero-normal-velocity boundary condition on  $r = a$  and the usual continuity and derivative-jump conditions across the source, it can be shown that

$$G_n = \begin{cases} \frac{1}{4} \exp(i\psi) \int_{-\infty}^{\infty} \left\{ Y_n(\gamma r) - \frac{Y'_n(\gamma a)}{J'_n(\gamma a)} J_n(\gamma r) \right\} J_n(\gamma r_1) \exp(ik(x - x_1)) dk \\ \frac{1}{4} \exp(i\psi) \int_{-\infty}^{\infty} \left\{ Y_n(\gamma r_1) - \frac{Y'_n(\gamma a)}{J'_n(\gamma a)} J_n(\gamma r_1) \right\} J_n(\gamma r) \exp(ik(x - x_1)) dk \end{cases} \quad (3.34)$$

for  $r_1 < r$  and  $r_1 > r$  respectively, with

$$\gamma^2 = \frac{(\omega - U_\infty k)^2}{c_0^2} - k^2, \quad (3.35)$$

and

$$\psi = -\omega t + n\theta. \quad (3.36)$$

We proceed to examine the far-field acoustic intensity directly upstream and downstream of the point source at  $r = r_1$ . The integrands in (3.34) possess an infinite number of simple poles at the zeros of  $J'_n(\gamma a)$ , which we denote by

$$j'_{ns} = \gamma_{ns} a, \quad s = 0, 1, 2, \dots, \quad (3.37)$$

and using the relation (3.35) between  $\gamma$  and  $k$  the corresponding poles in the complex  $k$ -plane are given by

$$k_{ns}^\pm = -\frac{\omega M_\infty}{c_0 \beta^2} \pm \frac{1}{\beta} \left( \frac{\omega^2}{\beta^2 c_0^2} - \frac{j'^2_{ns}}{a^2} \right)^{1/2}, \quad 0 \leq s \leq p \quad (3.38)$$

and

$$k_{ns}^\pm = -\frac{\omega M_\infty}{c_0 \beta^2} \pm i \frac{1}{\beta} \left( -\frac{\omega^2}{\beta^2 c_0^2} + \frac{j'^2_{ns}}{a^2} \right)^{1/2}, \quad s > p, \quad (3.39)$$

where  $p$  is the largest value of  $s$  such that the square root in (3.38) is real; the first  $p + 1$  poles are situated along the real axis. The residue corresponding to the  $s$ th zero of  $J'_n(\gamma a)$  is then given by the expression

$$\text{Res}(\gamma a = j'_{ns}) = -\frac{1}{4} \exp(i\psi) \frac{Y'_n(\gamma_{ns} a)}{a(d\gamma/dk) J''_n(\gamma_{ns} a)} J_n(\gamma_{ns} r_1) J_n(\gamma_{ns} r) \exp\left(ik_{ns}^\pm(x - x_1)\right), \quad (3.40)$$

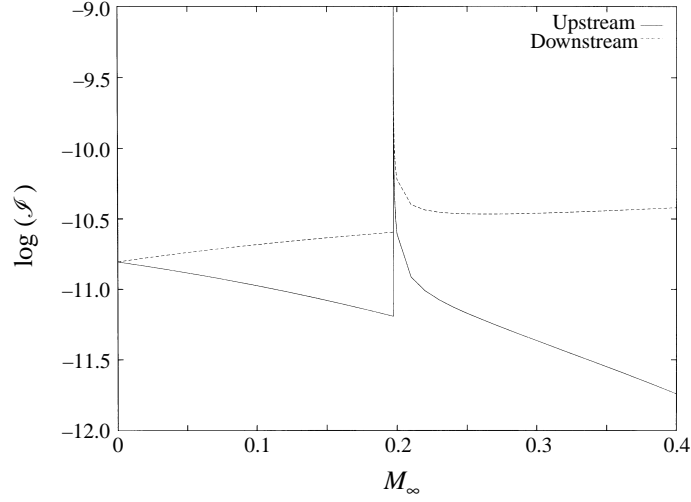


FIGURE 6. Predicted acoustic intensities upstream and downstream of the rotor for varying free-stream axial Mach number  $M_\infty$ . A cut-off condition exists at  $M_\infty = 0.197$ , and the intensity is predicted to be infinite there.

where

$$\frac{d\gamma}{dk} = -\frac{1}{\gamma} \left\{ (1 - M_\infty^2) k_{ns}^\pm + M_\infty \frac{\omega}{c_0} \right\}. \quad (3.41)$$

It then follows that the acoustic pressure within the duct due to the point source can be written as

$$p'(x, r; x_1, r_1) = \sum_{n,s} A_{ns} J_n(\gamma_{ns} r) \exp(-i\omega t + in\theta) \exp(ik_{ns}^\pm(x - x_1)) \quad (3.42)$$

where

$$A_{ns} = -\frac{1}{4a} \frac{Y_n'(\gamma_{ns} a)}{(d\gamma/dk) J_n'(\gamma_{ns} a)} J_n(\gamma_{ns} r_1), \quad (3.43)$$

and  $d\gamma/dk$  is given by (3.41). The axial component of the total acoustic intensity  $\mathbf{I}$  is given by (Morfey 1971; Goldstein 1976, p. 41)

$$\mathbf{I} \cdot \mathbf{x} = \left( \frac{p'}{\rho_0} + U_\infty u' \right) \left( \rho_0 u' + \frac{p'}{c_0^2} U_\infty \right), \quad (3.44)$$

where  $u'$  is here the unsteady axial velocity, and using (3.42) we deduce the mean acoustic intensity integrated across the cylinder cross-section,  $\mathcal{I}$ , in the form

$$\mathcal{I} = \frac{2\pi}{\rho_0} \sum_{n,s} \left\{ 1 + \frac{k_{ns}^\pm U_\infty}{\omega - U_\infty k_{ns}^\pm} \right\} \left\{ \frac{k_{ns}^\pm}{\omega - U_\infty k_{ns}^\pm} + \frac{U_\infty}{c_0^2} \right\} |A_{ns}|^2 \frac{1}{2j_{ns}^2} \left[ j_{ns}'^2 - n^2 \right] J_n^2(j_{ns}), \quad (3.45)$$

where we have used an orthogonality relation between the Bessel functions as given on p. 291 of Luke (1962). Depending on the  $\pm$  signs in the expression, the acoustic field can be predicted upstream ( $-$ ) or downstream ( $+$ ) of the fan.

The predicted noise levels in (3.45) are plotted in figure 6 for the first harmonic of BPF, in which the contributions from  $n = \{-1, 0, 1\}$  in (3.45) have been included. Since  $n = m + lB$ , it can be seen from (2.42) that the dominant contribution to the radiated power arises from the lowest orders (essentially because the Bessel function

decays exponentially as  $n$  increases). The free-stream axial Mach number  $M_\infty$  is varied between 0 and 0.4, which is a realistic range for aircraft operating conditions. For  $M_\infty = 0$ , there is no free-stream uniform flow and therefore the acoustic intensity is the same both upstream and downstream of the source. As  $M_\infty$  is increased, the mean intensity upstream (which we denote by  $\mathcal{I}_U$ ) decreases steadily, whereas that downstream (denoted by  $\mathcal{I}_D$ ) increases. The downstream-travelling sound waves propagate in the same direction as the mean flow and hence they are also convected with the flow, thereby leading to a greater intensity than that experienced upstream. For stronger mean flows, the acoustic intensity  $\mathcal{I}_D$  is accordingly higher, and it is clear that the ratio  $\mathcal{I}_U/\mathcal{I}_D$  generally decreases steadily as  $M_\infty$  is raised. The predicted power radiated upstream from a fan can therefore be obtained as a fraction of the total power calculated using the free-space Green's function.

However, an obvious non-uniformity exists in figure 6 when the Mach number  $M_\infty = 0.197$ . This corresponds to the acoustic cut-off condition, in which the term  $d\gamma/dk$  (given in (3.41)) in the denominator of (3.45) becomes zero. This occurs when

$$k = -\frac{\omega M_\infty}{\beta^2 c_0}, \quad \gamma = \gamma_{ns} = \frac{j'_{ns}}{a} = \frac{\omega}{\beta c_0}, \quad (3.46)$$

and at this resonant condition the acoustic intensities both upstream and downstream are predicted to be infinite, although the ratio  $\mathcal{I}_U/\mathcal{I}_D$  remains finite and is equal to 1. It is straightforward to deduce from (3.46) that 6 modes in (3.45) are cut-on for  $M_\infty < 0.197$  for the  $n = 1$  term in the sum, and that a seventh mode becomes cut-on at  $M_\infty = 0.197$ . As  $M_\infty$  is increased beyond 0.4, additional modes are cut-on for each harmonic index  $n$ . Acoustic cut-off (or resonance) only appears at a discrete number of parametric conditions, and while the problem of exactly how the flow should be modelled at these conditions (particularly in the light of the conclusion in Majumdar & Peake 1996 that two-dimensional strip theory is inapplicable at such resonances) requires further investigation, the theory derived in this paper holds for the vast majority of low-speed conditions, in which the duct modes are not close to cut-off.

## 4. Results

The theory presented in §§2 and 3 has been developed to provide analytical expressions for the important quantities at each stage of the unsteady distortion interaction process and the subsequent noise scattered to the far field. A parametric study is conducted in this section, and the results presented here display the spectra of the free-stream turbulence, the unsteady blade forces and the power and directivity of the radiated noise. It is also possible to investigate the behaviour of quantities such as the distorted wavenumber components at the fan or the unsteady pressure distribution along the rotating fan blades.

### 4.1. Intake geometry in static tests

In static tests a bellmouth (or flared) inlet is often attached to the front of the engine, and we can extend our theory to cover this case by representing this device by an actuator disk to model the inflow in a realistic manner. An actuator disk of radius  $r_B$  is placed at the cross-section of the bellmouth rim and the flow at the fan, downstream of the flared intake, is then taken to be uniform and parallel. The constant axial speed

$U_B$  at the actuator disk is calculated using the simple conservation-of-mass relation

$$U_B = \frac{r_f^2 U_f}{r_B^2}, \quad (4.1)$$

where  $U_f$  and  $r_f$  are the axial flow speed and duct radius at the fan (with  $r_B > r_f$ ). The strength of the actuator disk can be determined from  $U_B$ , and by using a standard result (Glauert 1959, p. 202) for the axial flow at the actuator disk we find that

$$U_B = U_\infty + \frac{1}{2}U_d. \quad (4.2)$$

We compute the drift function and its radial derivative at the actuator disk (i.e. the bellmouth inlet), which is reasonable since the variation of the drift between the inlet and the fan is negligible. A justification of this simplification is presented in §5.2 of Majumdar (1996). We do not use the actuator disk model for any blade loading or sound radiation calculations; the sole use of the actuator disk is to provide a realistic description of the inflow which captures the essential features of the streamtube contraction. In static tests, it is ensured that the airflow conditions through the fan best represent those that occur in flight, and we accordingly take the same value of  $U_f$  in both static and flight conditions throughout our computations.

In flight, no such flared intakes are used and we use either an open rotor for our calculations, which is represented by an actuator disk of the same radius as the rotor, or the ducted rotor as described in §3.

#### 4.2. Turbulence spectra at the fan face

The results presented here are based on the theory described in §2.3 for an open rotor, although similar results exist for a ducted rotor. As is evident from the expression of the von Kármán spectra in (2.4), the key variables are the integral lengthscale  $L$  and the mean kinetic energy  $u_{\infty,1}^2$  of the turbulence. The latter quantity is simply a constant multiplicative factor which comes out of the integral expression for the spectra of the distorted turbulence, so we concentrate on the dependence on integral lengthscale.

The turbulence spectra effectively represent the turbulent kinetic energy for a range of frequencies  $\omega$ , where  $\omega = k_x U_\infty$ . Figure 7 displays the spectrum  $S_{xx}^{-26}(\omega)$  at a fixed point on the fan under typical static conditions, for varying integral lengthscales. The number of blades on typical fans varies between 22 and 30, and so for definiteness we choose an average value of  $B = 26$ , so that the value  $m = -26$  will be important in the contribution to tonal noise, as will be shown in §4.4. It is evident from figure 7 that for low wavenumbers (i.e. low frequencies) the turbulent energy increases as the integral lengthscale is raised, until we reach lengthscales greater than the order of the streamtube radius, beyond which the energy decreases as  $L$  is increased. It has been suggested by Ganz (1980) that eddies of integral scale larger than the streamtube radius are only slightly affected by the flow contraction, and as shown in figure 2 the streamtube radius is roughly 10 times the blade radius in indoor static conditions. In static tests, it is therefore not necessary to investigate the effects of free-stream turbulent fields with integral lengthscales of the same order as the streamtube radius. At higher axial wavenumbers (i.e. higher frequencies), we can see from figure 7 that the energy decays exponentially.

The difference in the form of turbulence spectra in static and flight conditions is also evident from figure 7. In flight, the energy level is observed to be higher and it also remains constant for a greater frequency range than under static conditions, before



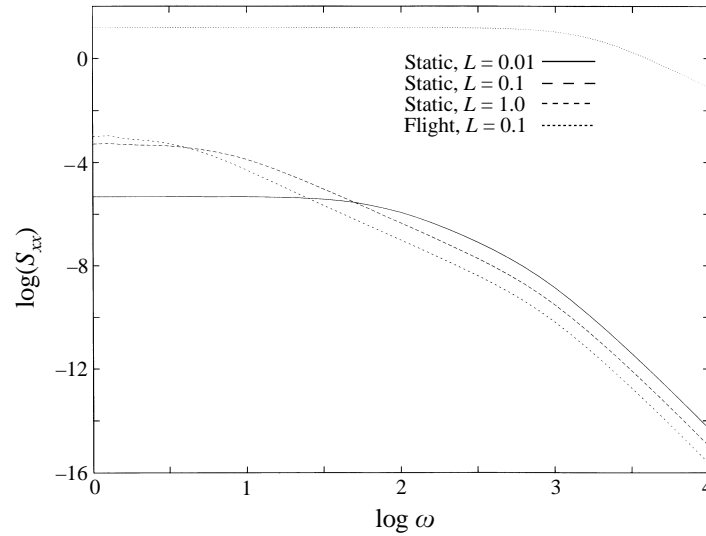


FIGURE 7. Turbulence spectra  $S_{xx}^{-26}(\omega)$  at the fan face, under typical static and flight conditions. Under static conditions we have  $U_d/U_\infty = 72.6$ , whereas in flight  $U_d/U_\infty = 0.82$ . The integral lengthscale  $L$  of the free-stream turbulence is varied.

decaying exponentially for higher wavenumbers. It is worth noting that the spectrum in flight is similar in shape to that obtained for the lowest value of  $L$  ( $L = 0.01$ ) in figure 7 under static conditions, i.e. the frequency at which the turbulent energy level starts to decay exponentially is roughly the same. With a suitable scaling of  $u_{\infty,1}^2$ , the spectra can be made to look identical. One of the key questions in static noise tests is how flight conditions can be reasonably simulated via the implementation of turbulence control mechanisms, and it is evident from figure 7 that the reduction of integral lengthscales and the mean energy of the free-stream turbulence in static conditions may lead to similar forms of distorted turbulence at the fan face to those expected in flight.

#### 4.3. Unsteady blade forces

In this subsection we present results for the unsteady blade forces arising from the interaction of the rotating fan and the distorted turbulent field at the fan face. In figure 8 the spectra for the unsteady blade forces  $S_{\Delta p \Delta p}(\mathbf{x}; \omega)$ , as expressed in (2.32), are displayed for varying integral lengthscales of the free-stream turbulence and under static and flight conditions. The circumferential harmonics of the turbulent field  $m = -27, -26, -25$  are considered here, since these values will be important in the prediction of tonal noise at blade passing frequency (see the next subsection). It is clear that peaks exist at  $\omega = -m\Omega$  for the values of  $m$  considered here, where  $\Omega$  is the shaft rotational frequency. The peaks are of higher magnitude for larger integral lengthscales  $L$ , and also of narrower width. The physical explanation is that each elongated eddy is chopped as each fan blade passes through it, providing a coherent unsteady forcing on the blade. Eddies of larger integral lengthscale are longer after distortion than those of smaller integral scale, and hence are chopped a greater number of times, thereby producing higher blade pressure levels at the harmonics of the shaft frequency. The spectra of the very small-scale eddies possess relatively low peak levels at harmonics of the shaft rotational frequency due to the limited chopping of distorted eddies of short axial extent, but the broadband part of the spectrum is

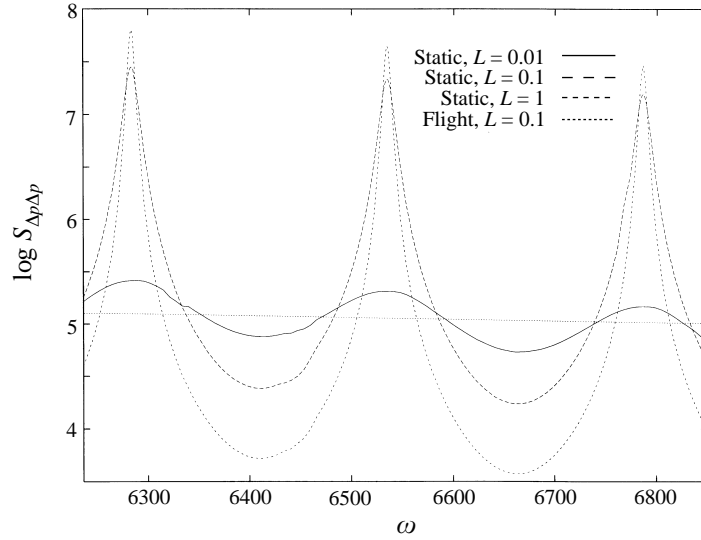


FIGURE 8. Spectra of blade forces  $S_{\Delta p \Delta p}(\mathbf{x}; \omega)$  at a fixed point on the blade, for different values of  $L$ . Harmonics at  $-m\Omega$  for  $m = -27, -26, -25$  are evident for static conditions, but are absent in flight. The spectrum corresponding to flight conditions is multiplied by a suitable value of  $\overline{u_{\infty,1}^2}$  in order to demonstrate that the effects of flight conditions may be mimicked by the ingestion of small-scale eddies in static tests. The values of  $U_\infty$  and  $U_d$  are as given in figure 7.

more significant than for higher lengthscales. The latter phenomenon is due to the presence of the three-dimensional von Kármán spectra  $S_{xx}^\infty(\mathbf{k})$  in the expression for  $S_{\Delta p \Delta p}(\mathbf{x}; \omega)$  (given in (2.32)), and if we examine the behaviour of  $S_{xx}^\infty(\mathbf{k})$  in figure 7 for large axial wavenumber  $k_x$  (corresponding to the broadband component), we observe that the value of  $S_{xx}^\infty(\mathbf{k})$  decreases slightly as  $L$  is raised. Conversely, the turbulent energy increases with  $L$  in cases when the axial wavenumber  $k_x$  is small.

A comparison between blade pressure spectra in typical static and flight conditions is also presented in figure 8, with the value of  $\overline{u_{\infty,1}^2}$  accordingly scaled to emphasize the similarity of flight effects and the interaction of small-scale eddies with the fan in static conditions. No peaks are observed to occur in flight, which highlights the lack of strong unsteady distortion, due to the forward motion of the aircraft. The consequence is that turbulent eddies are not significantly elongated as they are drawn towards the fan, and the turbulence that interacts with the fan is more or less isotropic. The eddies at the fan are therefore of relatively short axial extent, and due to the higher mean flow speed they are convected through the fan sufficiently quickly to avoid any repeated chopping. Only a weak, broadband unsteady loading therefore occurs on the blades.

#### 4.4. Open rotor radiation

Predictions of the radiated noise at a point  $\mathbf{x} \equiv (\sigma_0, \varphi)$  (displayed in figure 3) in the far field are presented in this subsection for the open rotor geometry, using the expression for the spectrum of the radiated power given in (2.46). The quantities within the integrand of (2.46) are evaluated at discrete values of  $r_1, x_1, r'_1$  and  $x'_1$ , and the unsteady blade pressure distribution  $\mathcal{L}_m$  along  $n_x$  chordwise points is calculated at a finite number  $n_r$  of radial stations  $r_1, r'_1$ . Values of  $n_x = 6$  and  $n_r = 5$  were found to give satisfactory results. Each integral over the spatial coordinates is performed using a

third-order finite-difference method, whereas the integral over the radial wavenumber is calculated numerically using a standard integration subroutine. The quantities  $B_{xi}^m$  which are dependent on the distorted field terms can be assumed to be independent of axial stations  $x_1, x_1'$ , since the drift function and basic flow streamfunction do not vary significantly over the blade chord, and therefore their values can be taken at the leading edge of the fan. Results are obtained for the radiated power in the far field for the whole range of observer angles  $\varphi$ . In our study, we concentrate on the frequency range containing the first two harmonics of blade passing frequency (BPF).

In figure 9(a) the power level (PWL), defined in (2.48), is plotted against the frequency  $\omega$  for typical indoor static testing conditions. The PWL is presented for different integral lengthscales  $L$  of the free-stream turbulence, and in each case there is a significant peak at the first two harmonics of BPF. The peak level is seen to increase, and the bandwidth of the peaks decrease, with increasing  $L$ , and the reason for this is precisely the same as given in § 4.3, i.e. that the elongated eddies with larger values of  $L$  are chopped more often in their passage through the fan. In fact, an infinitely long eddy would be chopped an infinite number of times, leading to a peak of  $\delta$ -function form with infinite amplitude and infinitesimal width. The peak width is observed to decrease as  $L$  is increased, and using dimensional arguments the width of each peak is expected to vary approximately in the manner

$$\Delta\omega \sim \frac{U_\infty}{L} \quad (4.3)$$

in cases where all other quantities remain fixed (some further investigation is required theoretically and experimentally to obtain a more detailed estimate for the peak width than is given in equation (4.3)).

The power level at the first two harmonics of BPF is displayed in figure 9(b) for varying integral lengthscale  $L$  (plotted on a log scale), under identical static testing conditions to those applied in figure 9(a). The radiated power at each harmonic of BPF increases as  $L$  is increased from zero, and it attains a peak when  $L$  is of order 0.1 m, and as  $L$  is increased further the PWL decreases slowly. In addition, we note that the magnitude of the tone at the first and second harmonic of BPF is similar for smaller  $L$ , whereas the first harmonic of BPF is approximately 11.5 dB higher than the second harmonic when  $L$  is approximately 1 m. In static tests, the first harmonic of BPF is known to represent the dominant source of fan noise, and this is consistent with our prediction shown in figure 9(b).

The significant difference in sound radiation between typical static and flight conditions is observed in figure 10(a), for the same integral lengthscale  $L$  in both cases. It is noticeable that in flight no peaks are apparent at either harmonic of BPF, and this is of course because no peaks in the blade pressure spectrum were observed in flight (see figure 8).

In figure 10(a) we see that the shape of the broadband component of the spectrum in flight is similar to that evaluated for static conditions. However, the power level is far greater in flight, as also found by Amiet, Simonich & Schlinker (1990). The reason behind this is not entirely obvious, so we will now discuss the phenomenon in some detail. We first note that the axial flow speed at the fan is the same under both static and flight conditions, so there is no difference in the energy input from the steady mean flow between the two conditions. The difference in the magnitude of the broadband noise must therefore be attributed to the form of the turbulence at the fan face. From (2.45), we notice that  $k_x$  is inversely proportional to the free-stream flow speed  $U_\infty$ , which we take to be 85 times larger in flight than in static conditions, and

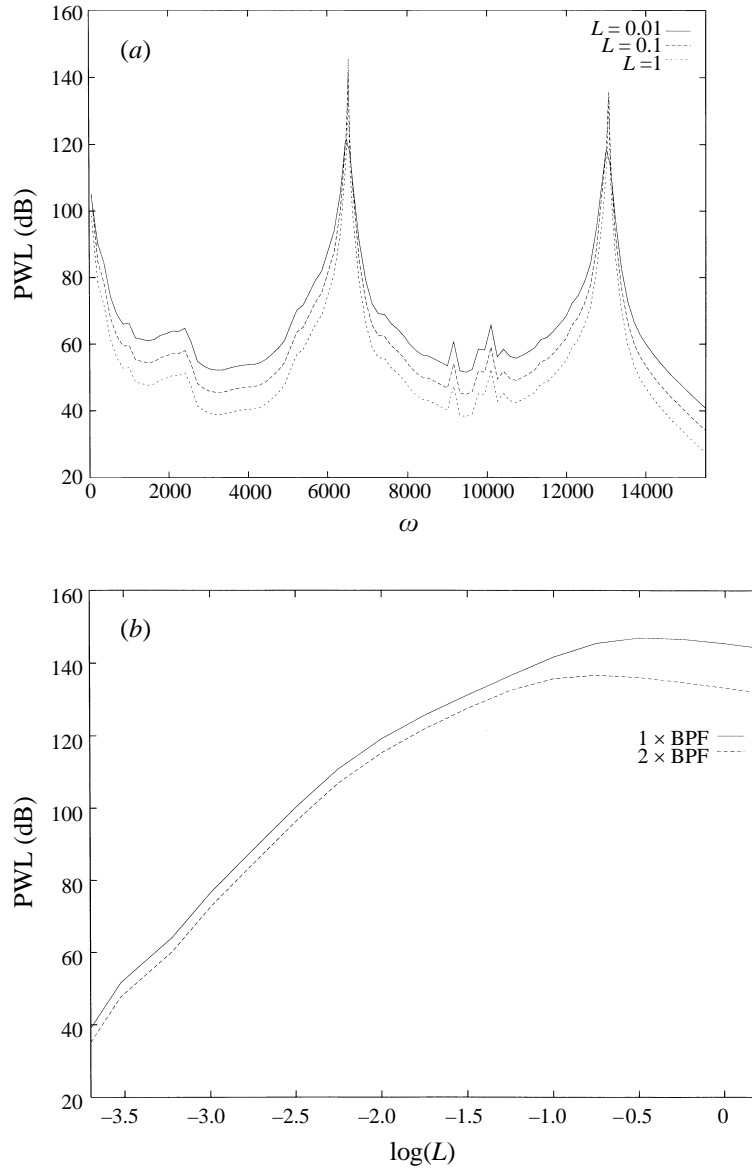


FIGURE 9. (a) Sound spectra under typical indoor static conditions (with  $U_d/U_\infty = 72.6$ ) for various values of turbulence integral lengthscale  $L$ . (b) Variation of tonal magnitude at the first and second harmonics of BPF with the integral lengthscale  $L$ , for indoor static conditions.

we therefore have a ratio of 85 between the axial wavenumber for each case. From (2.46), the quantity which changes most significantly with the axial wavenumber is the three-dimensional spectrum of the isotropic free-stream turbulence  $S_{ij}^\infty(\mathbf{k})$ , defined in (2.4). Since we are looking at the broadband spectrum, the value of  $k_x$  is quite large, especially under static conditions, and therefore the  $k_x^2$  term becomes dominant in the denominator of (2.4). In static conditions we therefore obtain a  $k_x^{-17/3}$  decay in the  $S_{xx}^\infty$  term, and similarly strong decay rates in  $S_{xr}^\infty$  and  $S_{rr}^\infty$  respectively (the decay in  $S_{xx}^\infty$  is shown in figure 10b), and there is therefore a ratio of roughly  $85^{11/3} \approx 10^7$

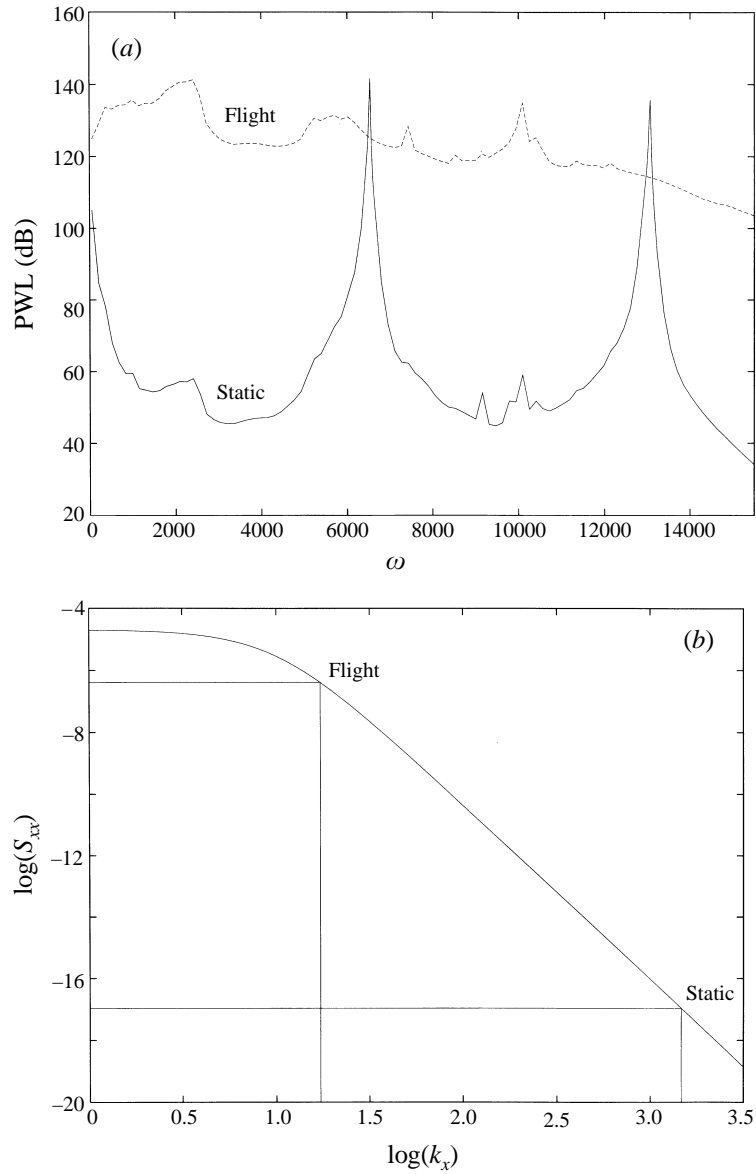


FIGURE 10. (a) Comparison between sound spectra in typical static conditions and flight, for  $L = 1$  m. (b) Behaviour of the  $S_{xx}^\infty$  component of the three-dimensional von Kármán spectra for  $\omega = 8000$  rad  $s^{-1}$  in (a). The transverse wavenumber component  $k_r = 10$  m $^{-1}$  here.

in the integrand of (2.46) between static and flight conditions. From figure 10(b), the incident turbulent energy in static conditions is observed to be much less than that in flight, and hence the broadband power level in the sound spectra is generally much lower than in flight. The difference is of order 70 dB, which is in agreement with the factor of  $85^{11/3}$ .

The directivity for an open rotor is predicted by (2.46), and a plot of the angular distribution of the sound power level for the first two harmonics of BPF is displayed in figure 11. The maximum sound occurs directly ahead of and behind the fan (i.e.

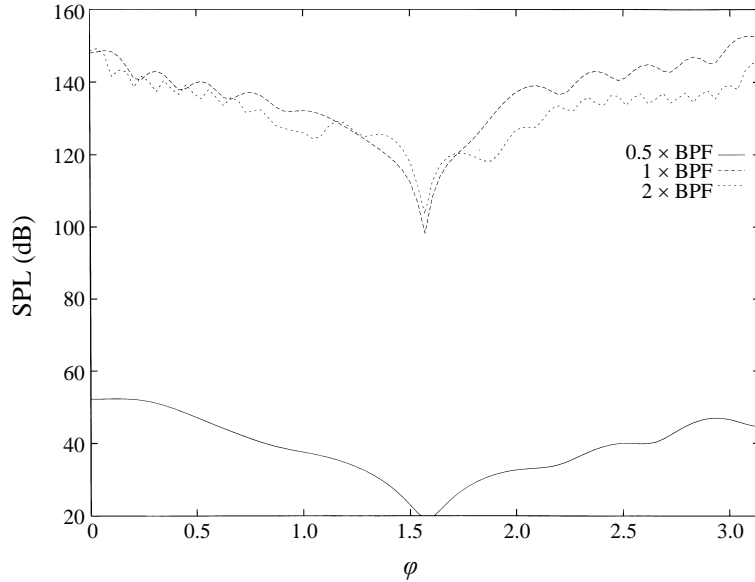


FIGURE 11. Directivity pattern for the first two harmonics of BPF and a broadband frequency  $\frac{1}{2} \times$  BPF under indoor static testing conditions (as in figure 9a).

along the engine axis), at angles  $\varphi = 0$  and  $\varphi = \pi$  respectively. A minimum occurs at right angles to the engine axis, at  $\varphi = \pi/2$  in each case. For most angles the scattered sound is greater at BPF than for its second harmonic. For comparison, the directivity of a broadband noise component at  $\frac{1}{2} \times$  BPF is shown and the noise level is accordingly lower at all angles, although a similar directivity pattern to those for the harmonics of BPF exists.

#### 4.5. Ducted rotor radiation

In figure 12, the power spectra for an aircraft in flight are presented for an unducted rotor and a ducted rotor. The methods to calculate the far-field radiated power using a Green's function approach are identical in both cases, and it is simply the inflow velocity fields that are of different form. The same parameters have been used for both cases. The two forms of the power spectra are shown to be very similar, with the radiated power from the unducted rotor being marginally greater overall. A possible explanation for the slightly higher noise level is that the distortion is greater for an open rotor, due to a larger streamtube radius. Some fluid particles which normally pass through an open rotor near the tip may be obstructed if a duct is inserted, and therefore the upstream catchment area (i.e. the streamtube radius) of fluid particles is smaller for the ducted rotor. From the total power calculated for a ducted rotor as displayed in figure 12, we would be able to predict the power radiated upstream of the ducted rotor using the results obtained in §3.3.

## 5. Concluding remarks

In this paper we have investigated the interaction between ingested atmospheric turbulence (known as 'unsteady distortion') and a rotating fan, in order to predict the resulting tonal and broadband noise in the far field. The key physical phenomena that occur in the distortion process can be briefly summarized. Owing to the high

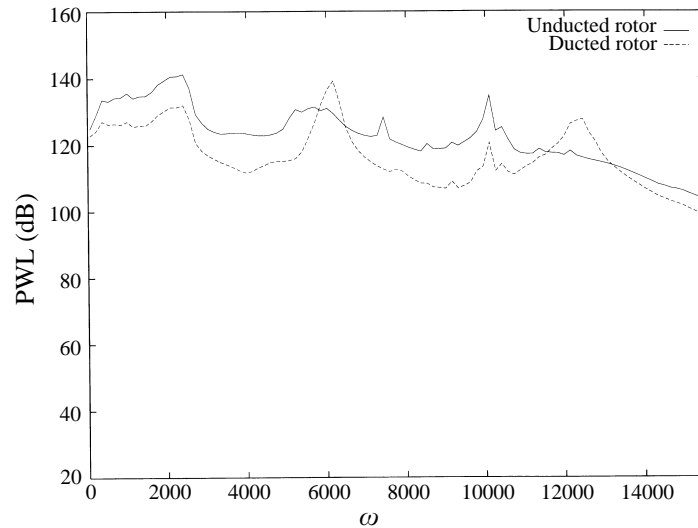


FIGURE 12. Spectra of the radiated power, calculated using the theories for an open rotor and a ducted rotor in flight ( $U_d/U_\infty = 0.82$ ).

angular speed of the fan, a streamtube contraction exists upstream which accelerates fluid elements towards the fan. In static conditions, the inflow contraction is very strong indeed whereas it is relatively weak in typical flight conditions of interest. Turbulent eddies in the atmosphere are drawn into the engine and elongated as they travel towards the fan. Although the free-stream turbulence is taken to be isotropic, the eddies that arrive at the fan in static conditions are of highly anisotropic form, with great elongation in the axial direction and a proportional contraction in the transverse direction. As each long, narrow filament is convected through the fan, it is repeatedly sliced by the rotating blades leading to a distribution of unsteady forces on the blades, thereby radiating sound to the far field.

The effects of typical static and flight (aircraft approach) conditions were analysed, as were the key parameters such as the integral lengthscale  $L$  of the free-stream turbulence. It was deduced that for integral lengthscales less than the streamtube radius, the unsteady distortion produced sharp tonal noise at harmonics of blade passing frequency under static conditions, with the magnitude of the tones increasing with  $L$  whereas the tonal width decreased as  $L$  was raised. In flight, the turbulent eddies underwent a very weak distortion, thereby leaving the turbulence almost isotropic, and the relatively short streamwise lengthscale therefore led to an absence of pressure pulses on the blades and hence no tones at harmonics of BPF were apparent in the spectra of the radiated sound.

There is great scope for further work on the theory of unsteady distortion noise. Our theory has been developed for an arbitrary form of free-stream atmospheric turbulence, although we have only used the most straightforward available model in the first instance. Firstly, the development of realistic turbulence models in static and flight conditions is required in order to quantify the precise effects of flight on the distortion, which will in turn enable the implementation of better inflow control devices in engine tests. The inclusion of more realistic steady flow fields upstream of the fan will also be necessary in due course, for both static conditions (in which the flared intake is added) and in flight. Furthermore, a significant improvement

to the theory for ducted-rotor radiation would be possible using the application of Chapman's (1996) theory to predict the directivity of sound. It will be a natural addition to our analysis, since it is able to predict noise levels from a ducted rotor directly from those obtained for an open rotor, via calculations of 'nil-shielding' directions and a subsequent open-to-ducted transfer function. The theory may also be coupled with a theoretical prediction scheme for 'steady distortion noise', which incorporates effects such as that of the non-uniform cross-section of the intake (known as 'droop'). Additionally, our theory can be extended to include effects such as swirl in the mean flow.

A significant part of the theory for unsteady distortion noise is based on ideas (Cargill 1993) originally outlined by the late A. M. Cargill of Rolls-Royce plc. The authors are grateful to Dr A. B. Parry for helpful discussions. S. J. Majumdar acknowledges financial support provided by EPSRC and Rolls-Royce plc under the CASE award scheme.

#### Appendix A. Basic steady flow field for the generalized actuator disk

The induced axial speed  $u(x, r)$  can be expressed in two forms which give identical results, and both are convenient for use in our analysis. The first expression is the more straightforward for calculation of  $u$  itself, but we also need certain derivatives of  $u$  to calculate the drift function of the basic flow, in which case it is simpler to use the second expression. The two forms for  $u(x, r)$  induced by an actuator disk of radius  $r_A$  are given by (Hough and Ordway 1965)

$$u(x, r) = \begin{cases} \frac{U_d}{4} \left[ \frac{x}{\pi(r_A r)^{1/2}} Q_{-1/2}(\omega) + A_0(\beta, \kappa) + 2 \right] & \text{if } [r \leq r_A] \\ \frac{U_d}{4} \left[ \frac{x}{\pi(r_A r)^{1/2}} Q_{-1/2}(\omega) - A_0(\beta, \kappa) \right] & \text{if } [r > r_A], \end{cases} \quad (\text{A } 1)$$

or alternatively

$$u(x, r) = \begin{cases} \frac{U_d x}{2\pi U_\infty r^{3/2}} \int_0^{r_A} \frac{1}{r_v^{1/2}} Q'_{-1/2}(\omega_1) dr_v & \text{if } [r > r_A] \text{ or } [r \leq r_A \text{ and } x < 0] \\ U_d + \frac{U_d x}{2\pi U_\infty r^{3/2}} \int_0^{r_A} \frac{1}{r_v^{1/2}} Q'_{-1/2}(\omega_1) dr_v & \text{if } [r \leq r_A \text{ and } x > 0], \end{cases} \quad (\text{A } 2)$$

where

$$\omega_1 = 1 + \frac{x^2 + (r - r_v)^2}{2rr_v}, \quad (\text{A } 3)$$

$Q_v(\omega)$  is the Legendre function and  $\omega$  is obtained by replacing  $r_v$  with  $r_A$  in (A3). The quantity  $U_d$  is the limit of  $u(x, r)$  at downstream infinity (i.e.  $x \rightarrow \infty$ ), where the flow is uniform and purely in the axial (streamwise) direction. The ratio  $U_d/U_\infty$  determines the strength of the inflow contraction, and as this quantity is increased the turbulent eddies experience a greater distortion. At the actuator disk itself, i.e.  $x = 0, r < r_A$ , the induced axial flow speed is  $u(0, r) = U_d/2$  and a non-zero radial component exists, so the flow is non-parallel as it approaches the disk.

The radial component of the induced flow takes the more straightforward form

$$v(x, r) = -\frac{U_d}{2\pi} \left( \frac{r_A}{r} \right)^{1/2} Q_{1/2}(\omega). \quad (\text{A } 4)$$



The corresponding streamfunction of the induced flow  $\Psi'(x, r)$  can be expressed as

$$\Psi' = \begin{cases} \frac{U_d x r}{2\pi} \left\{ -\frac{E(\kappa)}{\kappa} \left(\frac{r_A}{r}\right)^{1/2} + \frac{\kappa(x^2 + 2r_A^2 + 2r^2)K(\kappa)}{4(r_A r^3)^{1/2}} \right\} + \frac{U_d}{4} \left\{ r^2 - \frac{|r_A^2 - r^2|A_0(\beta, \kappa)}{2} \right\} \\ \frac{U_d x r}{2\pi} \left\{ -\frac{E(\kappa)}{\kappa} \left(\frac{r_A}{r}\right)^{1/2} + \frac{\kappa(x^2 + 2r_A^2 + 2r^2)K(\kappa)}{4(r_A r^3)^{1/2}} \right\} + \frac{U_d}{4} \left\{ r_A^2 - \frac{|r_A^2 - r^2|A_0(\beta, \kappa)}{2} \right\} \end{cases} \quad (\text{A } 5)$$

for  $[r \leq r_A]$  and  $[r > r_A]$  respectively. The streamfunction of the total steady flow is then given by

$$\Psi(x, r) = \frac{1}{2}U_\infty r^2 + \Psi'(x, r). \quad (\text{A } 6)$$

The functions  $K(\kappa)$  and  $E(\kappa)$  are complete elliptic integrals of the first and second kind respectively and  $A_0(\beta, \kappa)$  is Heuman's Lambda function. Expressions for these functions are given in Abramowitz & Stegun (1972). The terms  $\kappa$  and  $\beta$  are defined by

$$\kappa = \left( \frac{4r_A r}{(r_A + r)^2 + x^2} \right)^{1/2}, \quad \beta = \arcsin \left\{ \frac{x}{((r_A - r)^2 + x^2)^{1/2}} \right\}. \quad (\text{A } 7)$$

## Appendix B. Calculation of radial derivative of the drift

We start by writing

$$X = U_\infty A(x, R) = x + \int_{-\infty}^x \left[ \frac{U_\infty}{\mathcal{U}_x(x', R)} - 1 \right] dx', \quad (\text{B } 1)$$

where

$$\mathcal{U}_x(x', R) \equiv U_x(x', r_s(x', R)) \quad (\text{B } 2)$$

is the axial flow speed expressed as a function of  $x'$  and  $R$ . The partial  $R$ -derivative of the drift function is then written as

$$\left. \frac{\partial}{\partial R} (U_\infty A) \right|_x = - \int_{-\infty}^x \frac{U_\infty (\partial \mathcal{U}_x / \partial R)(x', R)}{[\mathcal{U}_x(x', R)]^2} dx'. \quad (\text{B } 3)$$

Using the chain rule, the term in the numerator of the integrand is expressed as

$$\left. \frac{\partial \mathcal{U}_x}{\partial R} \right|_{x'} = \left. \frac{\partial U_x}{\partial r_s} \right|_{x'} \left. \frac{\partial r_s}{\partial R} \right|_{x'}. \quad (\text{B } 4)$$

Since we are holding  $x'$  constant, we can then write

$$\left. \frac{\partial r_s}{\partial R} \right|_{x'} = \frac{1}{(\partial / \partial r_s)(R(x', r_s))|_{x'}} = \frac{U_\infty R(x', r_s)}{r_s U_x(x', r_s)}. \quad (\text{B } 5)$$

To evaluate

$$\left. \frac{\partial U_x}{\partial r_s} \right|_{x'} \quad (\text{B } 6)$$

we first write

$$U_x(x', r_s) = U_\infty + u(x', r_s), \quad (\text{B } 7)$$

where  $u(x', r_s)$  is given in (A 2), and express  $u(x', r_s)$  in the form

$$u(x', r_s) = \begin{cases} r_s^{-3/2} f(x', r_s) & \text{if } [r > r_A] \text{ or } [r \leq r_A \text{ and } x < 0] \\ U_d + r_s^{-3/2} f(x', r_s) & \text{if } [r \leq r_A \text{ and } x > 0] \end{cases} \quad (\text{B } 8)$$

We then have for  $x < 0$

$$\left. \frac{\partial U_x}{\partial r_s} \right|_{x'} = r_s^{-3/2} \frac{\partial f}{\partial r_s} - \frac{3}{2} r_s^{-5/2} f(x', r_s), \quad (\text{B } 9)$$

and hence

$$\left. \frac{\partial}{\partial R} (U_\infty \Delta) \right|_x = U_\infty^2 R(x, r) \int_{-\infty}^x \frac{-r_s^{-5/2} \frac{\partial f}{\partial r_s} + \frac{3}{2} r_s^{-7/2} f(x', r_s)}{[U_\infty + u(x', r_s)]^3} dx'. \quad (\text{B } 10)$$

The function  $\frac{\partial f}{\partial r_s}$  is given by

$$\begin{aligned} \frac{\partial f}{\partial r_s} &= \frac{U_d x'}{2\pi U_\infty} \int_0^{r_A} \frac{1}{r_v^{1/2}} \frac{\partial \omega_1'}{\partial r_s} Q_{-\frac{1}{2}}''(\omega_1') dr_v \\ &= \frac{U_d x'}{2\pi U_\infty} \int_0^{r_A} \int_0^{\pi/2} \frac{3(r_s^2 - r_v^2 - x'^2)}{r_s^2 r_v^{3/2}} \left[ \frac{x'^2 + (r_s - r_v)^2}{r_s r_v} + 4 \sin^2 \alpha \right]^{-5/2} d\alpha dr_v. \end{aligned} \quad (\text{B } 11)$$

### Appendix C. Calculation of the spectrum of distorted turbulence

The two-point correlation between velocities at positions  $\mathbf{x}$ ,  $\mathbf{y}$  and with time difference  $\tau$  between them is defined to be

$$R_{ij}(\mathbf{x}, \mathbf{y}; \tau) = \left\langle u_i^*(\mathbf{x}, t) u_j(\mathbf{y}, t + \tau) \right\rangle, \quad (\text{C } 1)$$

and by noting that the only statistical quantities in the expression are the components of  $\mathbf{u}^\infty$ , the correlation tensor is then given by (using (2.19))

$$\begin{aligned} R_{ij}(\mathbf{x}, \mathbf{y}; \tau) &= \frac{1}{(2\pi)^6} \int_{\mathbb{R}^3} \int_{\mathbb{R}^3} \int_{\mathbb{R}^3} \int_{\mathbb{R}^3} \sum_{m'=-\infty}^{\infty} \sum_{m=-\infty}^{\infty} B_{ik}^{m'*}(\mathbf{x}; \mathbf{k}') B_{jl}^m(\mathbf{y}; \mathbf{k}) \\ &\quad \times \exp \left\{ -ik'_1 (X(\mathbf{x}) - U_\infty t) - im' \left( \theta_x - \tan^{-1} \left( \frac{k'_3}{k'_2} \right) + \frac{\pi}{2} \right) \right\} \\ &\quad \times \exp \left\{ ik_1 (X(\mathbf{y}) - U_\infty (t + \tau)) + im \left( \theta_y - \tan^{-1} \left( \frac{k_3}{k_2} \right) + \frac{\pi}{2} \right) \right\} \\ &\quad \times R_{kl}^\infty(\boldsymbol{\eta}) \exp(-i(\mathbf{k} - \mathbf{k}') \cdot \mathbf{x}' - i\mathbf{k} \cdot \boldsymbol{\eta}) d^3 \mathbf{k} d^3 \mathbf{k}' d^3 \mathbf{x}' d^3 \boldsymbol{\eta} \end{aligned} \quad (\text{C } 2)$$

where  $\theta_x$  and  $\theta_y$  are the azimuthal components of position vectors  $\mathbf{x}$  and  $\mathbf{y}$  respectively, and  $R_{kl}^\infty$  is the correlation tensor for the upstream, pre-contraction turbulence as defined in (2.2). The integral over  $\mathbf{x}'$  then reduces to  $(2\pi)^3 \delta(\mathbf{k} - \mathbf{k}')$ , and the integral over  $\boldsymbol{\eta}$  gives the spectrum of the correlation function  $S_{kl}^\infty(\mathbf{k})$ , defined in (2.3). We are interested in a single point measurement (i.e.  $\mathbf{x} = \mathbf{y}$ ), and we Fourier transform  $R_{ij}(\mathbf{x}, \mathbf{x}; \tau)$  to yield the spectrum tensor (averaged over the azimuthal coordinate  $\phi$ ) in the form

$$S_{ij}(\mathbf{x}; \omega) = \frac{4\pi^2}{U_\infty} \int_0^\infty \sum_{m=-\infty}^{\infty} B_{ik}^m(\mathbf{x}; \mathbf{k}) B_{jl}^m(\mathbf{x}; \mathbf{k}) S_{kl}^\infty(\mathbf{k}) k_r dk_r, \quad (\text{C } 3)$$

for our axisymmetric flow geometry. The frequency  $\omega$  is related to the axial wavenumber  $k_x$  in the form

$$\omega = k_x U_\infty. \quad (\text{C } 4)$$

In our axisymmetric geometry where there is no swirl, the azimuthal component of the basic steady flow is zero everywhere, and therefore the only non-zero components of  $B_{ij}^m(\mathbf{x}; \mathbf{k})$  are  $B_{xx}^m$ ,  $B_{xr}^m (= B_{rx}^m)$  and  $B_{rr}^m$ . We also note that these terms are all real (referring back to (2.18) and (2.20)). If we examine the sum over the indices  $k, l$  in (C 3), we observe that only the  $x$ - and  $r$ -components of  $S_{kl}^\infty(\mathbf{k})$  are required. Expressions for these terms using the von Kármán model for isotropic free-stream turbulence are given in (2.4).

#### REFERENCES

- ABRAMOWITZ, M. & STEGUN, I. A. 1972 *Handbook of Mathematical Functions*. Dover.
- AMIET, R. K. 1975 Acoustic radiation from an airfoil in a turbulent stream. *J. Sound Vib.* **41**, 407–420.
- AMIET, R. K. 1977 Noise produced by turbulent flow into a propeller or helicopter rotor. *AIAA J.* **15**, 307–308.
- AMIET, R. K., SIMONICH, J. C. & SCHLINKER, R. H. 1990 Rotor noise due to atmospheric turbulence ingestion. Part II: aeroacoustics results. *J. Aircraft* **27**, 15–22.
- BATCHELOR, G. K. & PROUDMAN, I. 1954 The effect of rapid distortion of a fluid in turbulent motion. *Q. J. Mech. Appl. Maths* **7**, 83–103.
- CARGILL, A. M. 1993 A theory of fan unsteady distortion noise. *Tech. Rep.* TSG0675. Rolls-Royce plc.
- CHAPMAN, C. J. 1996 Sound radiation from a cylindrical duct. Part 2. Source modelling, nil-shielding directions, and the open-to-ducted transfer function. *J. Fluid Mech.* **313**, 367–380.
- CONWAY, J. T. 1995 Analytical solutions for the actuator disk with variable radial distribution of load. *J. Fluid Mech.* **297**, 327–355.
- CRIGHTON, D. G. & PARRY, A. B. 1991 Asymptotic theory of propeller noise. Part II. Supersonic single-rotation propeller. *AIAA J.* **29**, 2031–2037.
- CUMPSTY, N. A. & LOWRIE, B. W. 1974 The cause of tone generation by aeroengine fans at high subsonic speeds and the effect of forward speed. *Trans. ASME: J. Engng for Power* **96**, 228–234.
- DEAN, L. W. 1971 Broadband noise generated by airfoils in turbulent flow. *AIAA Paper* 71-587.
- DOWLING, A. P. & FLOWCS WILLIAMS, J. E. 1983 *Sound and Sources of Sound*. Ellis Horwood Ltd.
- GANZ, U. 1980 Analytical investigation of fan tone noise due to ingested atmospheric turbulence. *Tech. Rep.* CR-2574. NASA.
- GLAUERT, H. 1959 *Aerofoil and Airscrew Theory*. Cambridge University Press.
- GOLDSTEIN, M. E. 1976 *Aeroacoustics*. McGraw-Hill.
- GOLDSTEIN, M. E. 1978 Unsteady vortical and entropic distortions of potential flows round arbitrary obstacles. *J. Fluid Mech.* **89**, 433–468.
- GRADSHTEYN, I. S. & RYZHIK, I. M. 1980 *Integrals of Bessel Functions*. Academic.
- HANSON, D. B. 1974 The spectrum of rotor noise caused by atmospheric turbulence. *J. Acoust. Soc. Am.* **56**, 110–126.
- HINZE, J. O. 1959 *Turbulence*. McGraw-Hill.
- HOMICZ, G. F. & GEORGE, A. R. 1974 Broadband and discrete frequency radiation for subsonic rotors. *J. Sound Vib.* **36**, 151–177.
- HOUGH, G. R. & ORDWAY, D. E. 1965 The generalised Actuator Disk. In *Developments in Theoretical and Applied Mechanics*, vol. II, pp. 317–336. Pergamon.
- HUNT, J. C. R. 1973 A theory of turbulent flow round two-dimensional bluff bodies. *J. Fluid Mech.* **61**, 625–706.
- HUNT, J. C. R. 1978 A review of the theory of rapidly distorted turbulent flows and its applications. *Fluid Dyn. Trans.* **9**, 121–152.
- JONES, D. S. 1966 *Generalised Functions*. McGraw-Hill.

- LEVINE, H. & SCHWINGER, J. 1948 On the radiation of sound from an unflanged circular pipe. *Phys. Rev.* **73**, 383–406.
- LIGHTHILL, M. J. 1956 Drift. *J. Fluid Mech.* **1**, 31–53.
- LUKE, Y. L. 1962 *Integrals of Bessel Functions*. McGraw-Hill.
- MAJUMDAR, S. J. 1996 Unsteady distortion noise. PhD thesis, University of Cambridge.
- MAJUMDAR, S. J. & PEAKE, N. 1996 Three-dimensional effects in cascade-gust interaction. *Wave Motion* **23**, 321–337.
- MANI, R. 1971 Noise due to interaction of inlet turbulence with isolated stators and rotors. *J. Sound Vib.* **17**, 251–260.
- MORFEY, C. L. 1971 Acoustic energy in non-uniform flows. *J. Sound Vib.* **14**, 159–170.
- MUGRIDGE, B. D. 1970 Sound radiation from airfoils in turbulent flow. *J. Sound Vib.* **13**, 362–363.
- NOBLE, B. 1958 *Methods Based on the Wiener-Hopf Technique*. Pergamon.
- PARRY, A. B. & CRIGHTON, D. G. 1989 Asymptotic theory of propeller noise. Part I. Subsonic single-rotation propeller. *AIAA J.* **27**, 1184–1190.
- PEAKE, N. 1995 On the radiation properties of an axisymmetric cylinder. *Wave Motion* **22**, 371–385.
- PRANDTL, L. 1933 Attaining a steady air stream in wind tunnels. *Tech. Rep.* TM 726. NACA.
- RIBNER, H. S. & TUCKER, M. 1953 Spectrum of turbulence in a contracting stream. *Tech. Rep.* 1113. NACA.
- SHARLAND, I. J. 1964 Sources of noise in axial flow fans. *J. Sound Vib.* **1**, 302–322.
- SIMONICH, J. C., AMIET, R. K., SCHLINKER, R. H. & GREITZER, E. M. 1986 Helicopter rotor noise due to ingestion of atmospheric turbulence. *Tech. Rep.* CR-3973. NASA.
- SIMONICH, J. C., AMIET, R. K., SCHLINKER, R. H. & GREITZER, E. M. 1990 Rotor noise due to atmospheric turbulence ingestion. Part I: fluid mechanics. *J. Aircraft* **27**, 7–15.
- SMITH, S. N. 1972 Discrete frequency sound generation in axial flow turbomachines. *Areo. Res. Counc. R & M* 3709. Ministry of Defence.
- TAYLOR, G. I. 1935 Turbulence in a contracting stream. *Z. Angew. Math. Mech.* **15**, 91–96.
- WHITEHEAD, D. S. 1987 Classical two-dimensional methods. In *Manual on Aeroelasticity in Axial-Flow Turbomachines : Unsteady Turbomachinery Dynamics AGARD-AG-298*, vol. 1.